



Cite this: DOI: 10.1039/d5md00251f

# Design, synthesis, and biological evaluation of novel *N*-(1*H*-indazol-6-yl)benzenesulfonamide derivatives as potent PLK4 inhibitors†

Pengkun Sun,<sup>‡a</sup> Cunzheng Fan,<sup>§a</sup> Nian Liu,<sup>¶a</sup> Minghui Tong,<sup>b</sup> Xuan Shi,<sup>b</sup> Han Wang,<sup>b</sup> Shuyi Mu,<sup>a</sup> Ningyuan Hu,<sup>a</sup> Yixiang Sun,<sup>a</sup> Haoyu Zhang,<sup>a</sup> Zixuan Gao,<sup>a</sup> Dongmei Zhao<sup>¶\*a</sup> and Maosheng Cheng<sup>¶a</sup>

PLK4 is a serine/threonine protein kinase situated at the centrosome, acting as a crucial regulatory element in the regulation of cell mitosis and significantly contributing to the preservation of genomic integrity. The overexpression of PLK4 is intricately linked to the onset and progression of several cancers, influencing a range of actions in tumor cells, such as proliferation, differentiation, migration, and invasion. PLK4 has been identified as a target for the therapy of several malignancies, especially breast cancer characterized by elevated *TRIM37* levels. Consequently, the development of safe, efficient, and highly selective PLK4 inhibitors is of considerable importance. This study examined existing PLK4 inhibitors, chose *N*-(1*H*-indazol-6-yl)benzenesulfonamide as the core structure, and synthesized a series of extremely effective PLK4 inhibitors by structural simplification and fragment growth methodologies. *In vitro* enzyme activity studies demonstrated that compound K22 has significant PLK4 inhibitory activity ( $IC_{50} = 0.1$  nM). K22 demonstrated significant anti-proliferative efficacy against MCF-7 breast cancer cells at the cellular level ( $IC_{50} = 1.3$   $\mu$ M). Moreover, PLK4 inhibitor K22 showed acceptable human liver microsome stability ( $T_{1/2} = 51.0$  min). In the pharmacokinetic study, compound K22 exhibited a good area under the curve ( $AUC_{0-t} = 447 \pm 47.6$  ng h mL<sup>-1</sup>) and acceptable half-life ( $T_{1/2} = 1.07 \pm 0.111$  h). In summary, compound K22 has further research value as a PLK4 inhibitor.

Received 21st March 2025,  
Accepted 13th May 2025

DOI: 10.1039/d5md00251f

rsc.li/medchem

## 1. Introduction

The process of cell mitosis is governed by numerous internal and external factors, and mitotic mistakes can result in various diseases, including neoplastic disorders.<sup>1</sup> PLK4 is a constituent of the highly conserved serine/threonine protein kinase family, which is involved in cell mitosis, DNA damage response, and the preservation of genomic stability.<sup>2,3</sup> There are five subtypes in this family: PLK1, PLK2 (Snk), PLK3 (Fnk/Prk), PLK4 and PLK5.<sup>4</sup> PLK4 is a major regulator of centriole replication during mitosis, found within centrioles;<sup>5</sup> its overexpression results in mitotic mistakes in cells and can generate cancer.<sup>6</sup> Since 2003, multiple studies have identified abnormal PLK4 expression in the majority of human tumors, including

breast cancer,<sup>7</sup> gastric cancer,<sup>8</sup> colon cancer,<sup>9</sup> bone cancer,<sup>10,11</sup> neuroblastoma,<sup>12</sup> melanoma,<sup>13</sup> cervical cancer,<sup>14</sup> hepatic cancer,<sup>15</sup> lung cancer,<sup>16</sup> and leukemia.<sup>17,18</sup> In September 2020, two articles in *Nature* reported that the inhibition of PLK4 leads to intracellular centrosome depletion and mitotic failure in malignancies with elevated *TRIM37* expression, suggesting that PLK4 inhibitors may facilitate targeted therapy for tumors with significant *TRIM37* amplification.<sup>19,20</sup> PLK4 inhibitors are reported to be synthetically lethal in tumors with elevated *TRIM37* amplification; the ablation of the PLK4 gene induces apoptosis in breast cancer cells while sparing normal cells.<sup>20</sup> Furthermore, xenograft studies in mice demonstrate that the loss of PLK4 markedly suppresses the proliferation of breast cancer tumor cells.<sup>21</sup> Consequently, the inhibition of PLK4 presents a novel approach to induce selective mitotic failure and offers a new treatment strategy for breast cancer characterized by significant *TRIM37* amplification.

To date, PLK4 inhibitors have mostly been classified into two types based on the central parent nucleus and the binding mechanism to the hinge region: indazoles and aminopyrazoles (Fig. 1). **Axitinib** is a *pan*-VEGFR inhibitor

<sup>a</sup> Key Laboratory of Structure-Based Drug Design and Discovery, Ministry of Education, School of Pharmaceutical Engineering, Shenyang Pharmaceutical University, 103 Wenhua Road, Shenhe District, Shenyang 110016, PR China. E-mail: medchemzhao@163.com

<sup>b</sup> 3D BioOptima, 1338 Wuzhong Avenue, Suzhou, 215104, China

† Electronic supplementary information (ESI) available. See DOI: <https://doi.org/10.1039/d5md00251f>

‡ First author.

§ Co-first author.

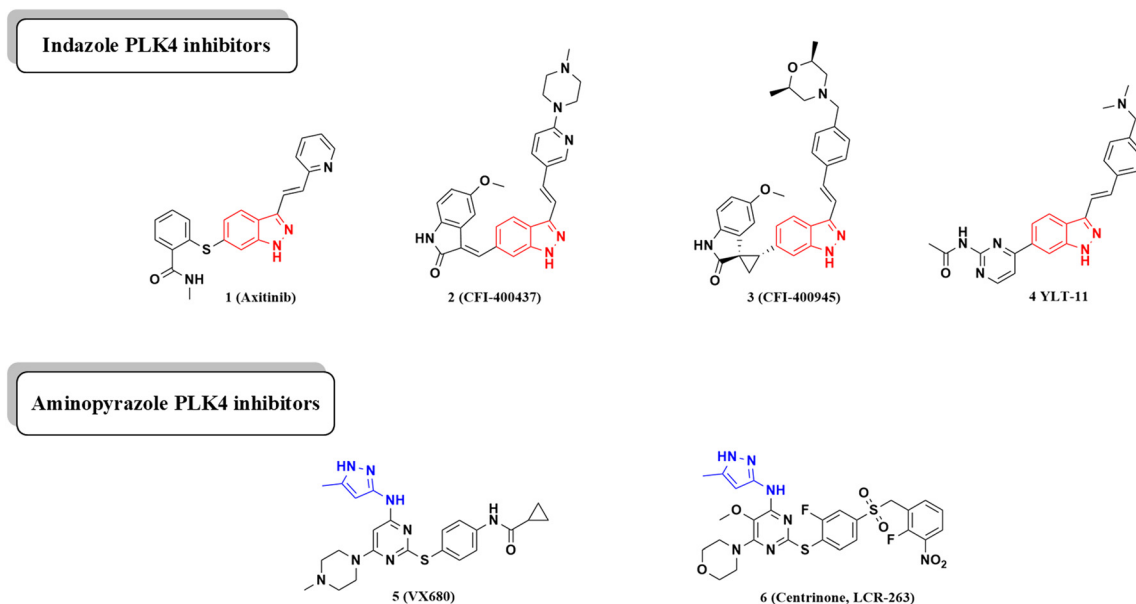


**Fig. 1** Classification of typical PLK4 inhibitors by the central scaffold and the binding mode between chemical structures and the hinge region.

that also exerts an inhibitory impact on PLK4 ( $IC_{50} = 6.5$  nM).<sup>22</sup> In 2014, Pauls *et al.* synthesized a set of indazole PLK4 inhibitors, namely **CFI-400437** and **CFI-400945**, with PLK4  $IC_{50}$  values of 0.6 nM and 2.8 nM, respectively.<sup>23</sup> It is worth mentioning that **CFI-400945** is currently the only PLK4 inhibitor in clinical phase II. Yu *et al.* used a framework transformation method to obtain **YLT-11** based on the structure of **CFI-400945**.<sup>24</sup> **VX680** was first introduced in 2004 as a generic inhibitor of aurora kinases<sup>25</sup> Concurrently,

reports indicated that **VX680** also inhibits PLK4, with a  $K_i$  value of 7.66 nM.<sup>26</sup> Oegema *et al.*, informed by a modeling study, utilized **VX680** as a template to create **centrinone** (**LCR-263**), a potent and selective PLK4 inhibitor (PLK4  $IC_{50} = 2.7$  nM), which led to p53-dependent cell cycle arrest in the G1 phase.<sup>27</sup>

In this section of the study, we examined the binding interactions of **axitinib**, **CFI-400945** and **YLT-11** with PLK4 (PDB code 4JXF). Molecular docking showed that the indazole

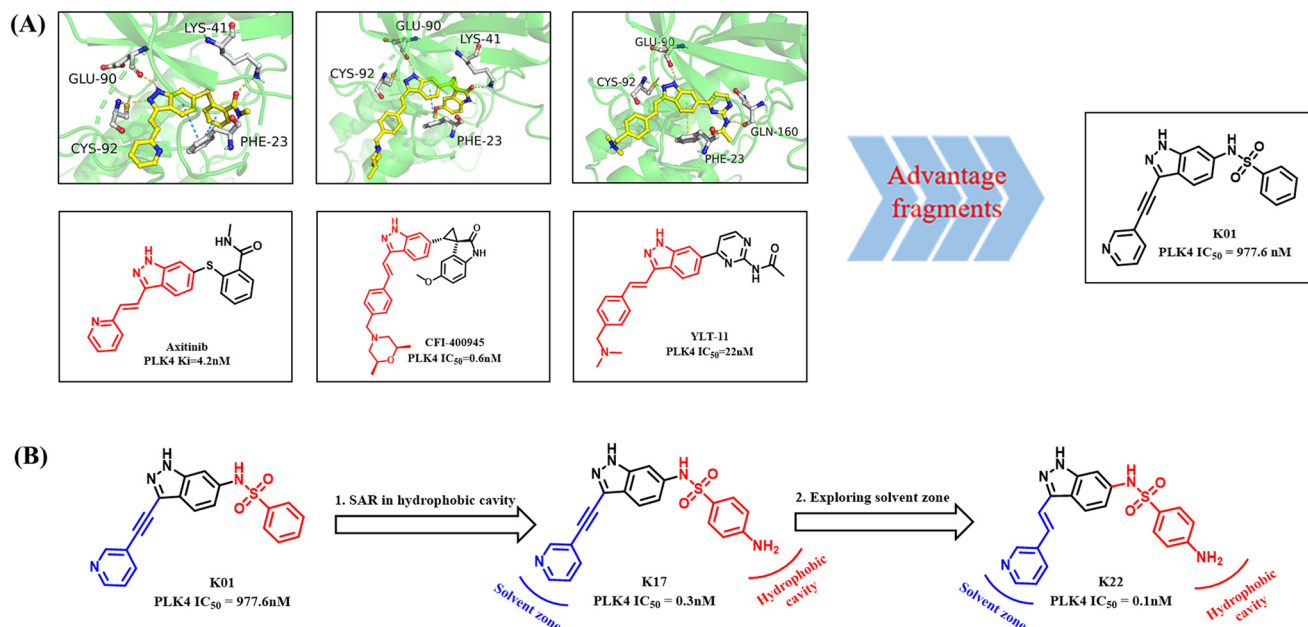
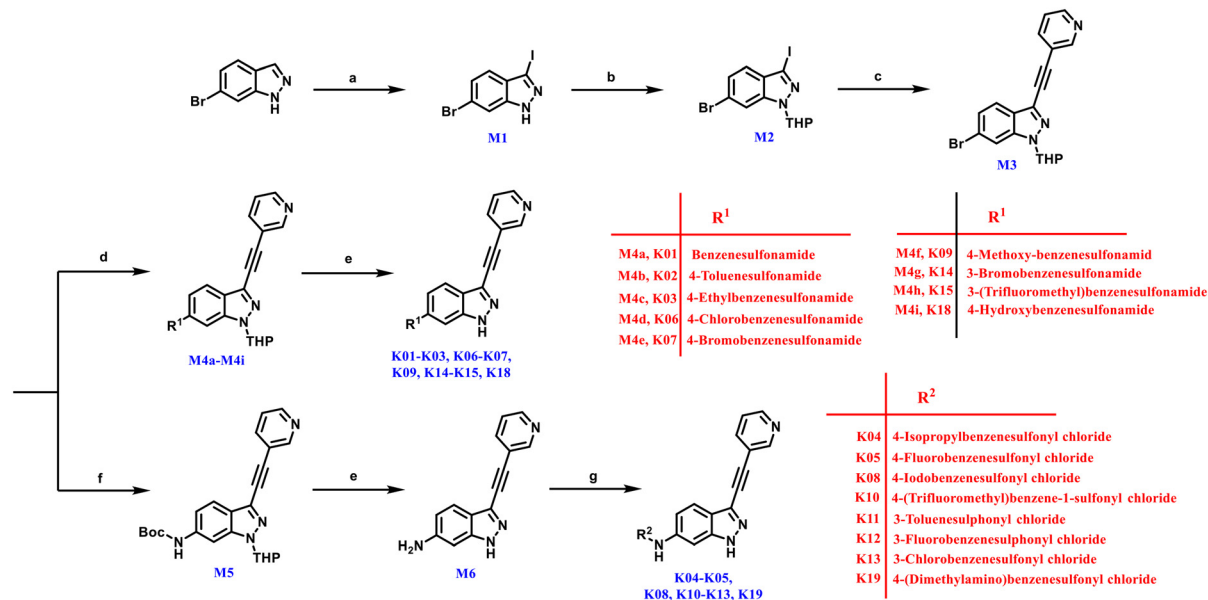


**Fig. 2** (A) Binding mode of **axitinib**, **CFI-400945** and **YLT-11** in the ATP-binding site of PLK4 (PDB code: 4JXF, colored green). Interactions are illustrated with yellow or blue dashed lines. The kinase is depicted in green cartoons. Ligands are depicted by the element with carbons in yellow. (B) Design strategies of novel Polo-like kinase 4 (PLK4) inhibitors.



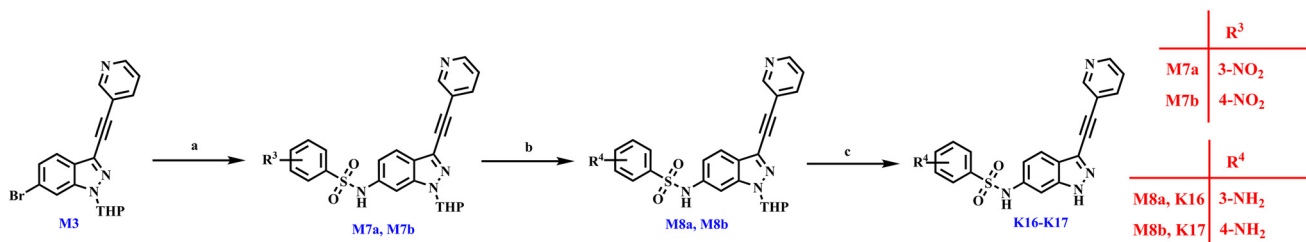
**Scheme 1** Synthesis of compounds **K01–K15** and **K18–K19**. Reagents and conditions: (a) NIS, DMF, r.t., 5 h; (b) DHP, *p*-toluenesulfonic acid, DCM, 0 °C then r.t., 4 h; (c) 3-ethynyl pyridine, CuI, Pd(PPh<sub>3</sub>)<sub>4</sub>, TEA, r.t., 5 h; (d) toluenesulfonamide and its derivatives, K<sub>2</sub>CO<sub>3</sub>, CuI, DMEDA, CH<sub>3</sub>CN, 100 °C, 12 h; (e) *p*-toluenesulfonic acid, MeOH:H<sub>2</sub>O = 3:0.5, 80 °C, 3 h; (f) *tert*-butyl carbamate, Cs<sub>2</sub>CO<sub>3</sub>, Pd<sub>2</sub>(dba)<sub>3</sub>, xantphos, 1,4-dioxane, 100 °C, 8 h; (g) benzenyl chloride derivatives, DMAP, pyridine, 0 °C then r.t., 5 h.

core of the three compounds forms important hydrogen bonds with the hinge region amino acid residues Glu-90 and Cys-92. Each compound also has parts that are hydrophilic and extend into the solvent region, and parts that are hydrophobic and extend into the DFG motif (Fig. 2). Consequently, we adopted a structural simplification strategy to retain the indole core as the backbone, connecting the pyridine through an alkyne to extend into the solvent region as a hydrophilic fragment. Subsequently, we introduced a benzenesulfonamide fragment to occupy the hydrophobic pocket close to the DFG motif. This led to the synthesis of compound **K01**, which demonstrates an inhibitory activity of 977.6 nM against PLK4 (Fig. 2A). And then, using **K01** as the lead compound, we introduced different substituents on the benzene ring and ultimately obtained compound **K17** (IC<sub>50</sub> = 0.3 nM), which exhibited excellent PLK4 inhibitory activity. What's more, we further modified the segment extending into the solvent region. Ultimately, we synthesized compound **K22** (IC<sub>50</sub> = 0.1 nM), which demonstrates significant PLK4 inhibitory action (Fig. 2B).

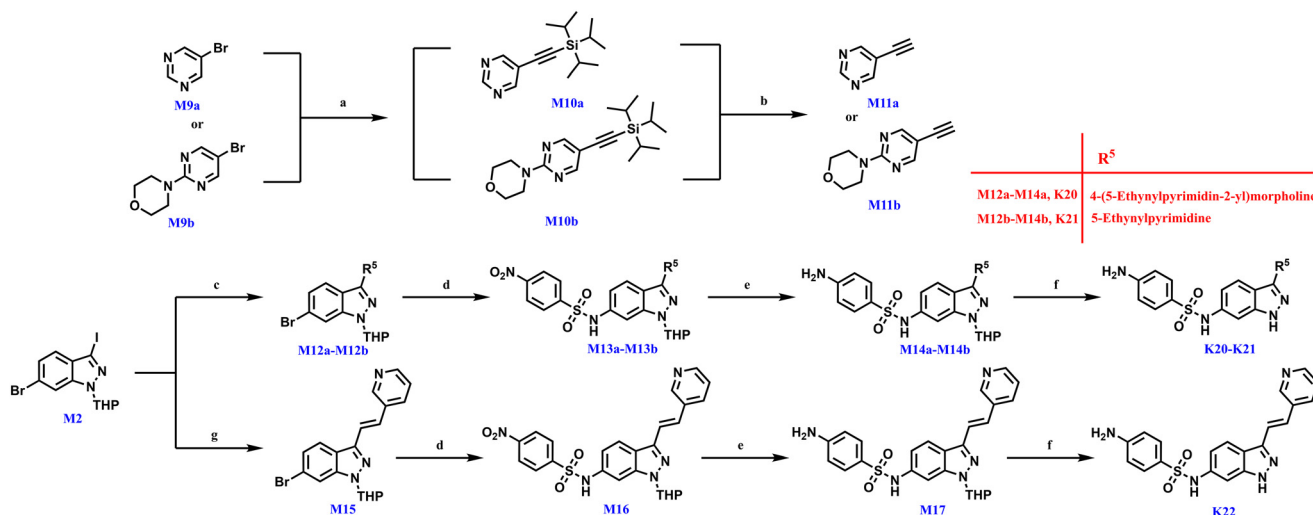
## 2. Results and discussion

### 2.1 Chemistry

Scheme 1 illustrates the synthetic pathway employed to synthesize molecules **K01–K15** and **K18–K19**. Beginning with commercially available 6-bromoindazole, it was treated with *N*-iodosuccinimide in a nucleophilic substitution reaction to yield intermediate **M1**. Subsequently, *p*-toluenesulfonic acid was used as a catalyst for the THP protection of **M1** using 3,4-dihydro-2*H*-pyran to get intermediate **M2**. Intermediate **M2** underwent a Sonogashira coupling reaction with 3-ethynylpyridine to provide crucial intermediate **M3**. Intermediate **M3** was reacted with different benzenesulfonamides by the Goldberg amination reaction to yield intermediates **M4a–M4i**. Ultimately, intermediates **M4a–M4i** were deprotected with *p*-toluenesulfonic acid, producing **K01–K03**, **K06–K07**, **K09**, **K14–K15**, and **K18**. Intermediate **M5** was synthesized from key intermediate **M3** and *tert*-butyl carbamate using a Buchwald–Hartwig coupling process, followed by deprotection with *p*-toluenesulfonic acid



**Scheme 2** Synthesis of compounds **K16–K17**. Reagents and conditions: (a) 3-nitrobenzenesulfonamide or 4-nitrobenzenesulfonamide, K<sub>2</sub>CO<sub>3</sub>, CuI, DMEDA, CH<sub>3</sub>CN, 100 °C, 12 h; (b) Fe, AcOH, MeOH:THF = 2:1, 60 °C, 4 h; (c) *p*-toluenesulfonic acid, MeOH:H<sub>2</sub>O = 3:0.5, 80 °C, 3 h.



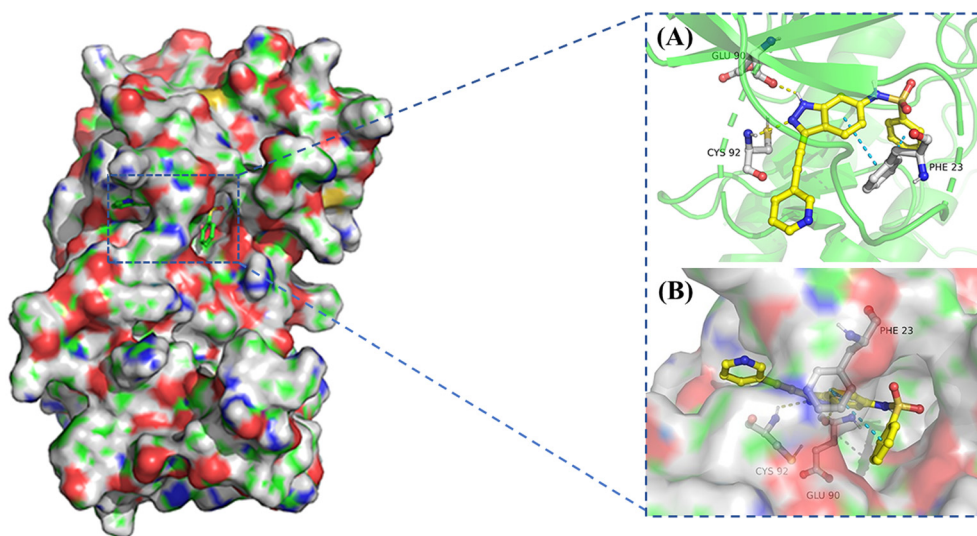
**Scheme 3** Synthesis of compounds **K20–K22**. Reagents and conditions: (a) (triisopropylsilyl)acetylene,  $\text{PPh}_3$ ,  $\text{Pd}(\text{OAc})_2$ , TEA,  $100^\circ\text{C}$ , 8 h; (b) TBAF, THF, r.t., 2 h; (c) **M11a** or **M11b**, CuI,  $\text{Pd}(\text{PPh}_3)_4$ , TEA, r.t., 5 h; (d) 4-nitrobenzenesulfonamide,  $\text{K}_2\text{CO}_3$ , CuI, DMEDA,  $\text{CH}_2\text{CN}$ ,  $100^\circ\text{C}$ , 12 h; (e) Fe, AcOH,  $\text{MeOH}:\text{THF} = 2:1$ ,  $60^\circ\text{C}$ , 4 h; (f) *p*-toluenesulfonic acid,  $\text{MeOH}:\text{H}_2\text{O} = 3:0.5$ ,  $80^\circ\text{C}$ , 3 h; (g) 3-ethynylpyridine, DIEA, tri(*o*-tolyl)phosphine,  $\text{Pd}(\text{OAc})_2$ , DMF,  $100^\circ\text{C}$ , 4 h.

to yield intermediate **M6**. Ultimately, compounds **K04–K05**, **K08**, **K10–K13**, and **K19** were synthesized using intermediate **M6** with several benzenesulfonyl chlorides under basic circumstances.

The synthesis of target compounds **K16–K17**, initiated from **M3**, is illustrated in Scheme 2. **M7a–M7b** were synthesized using the Goldberg amination process, wherein 3-nitrobenzene sulfonamide or 4-nitrobenzene sulfonamide reacted with **M3**. In the presence of iron powder and acetic acid, **M7a–M7b** were converted to **M8a–M8b**, which upon deprotection with *p*-toluenesulfonic acid produced **K16–K17**.

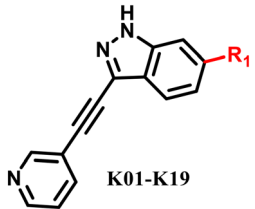
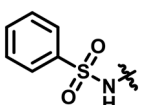
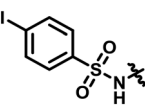
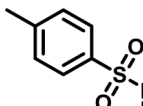
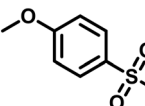
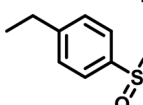
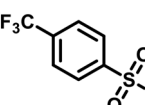
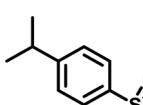
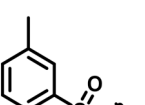
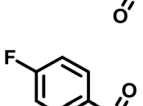
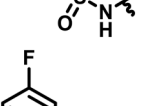
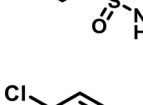
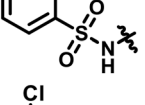
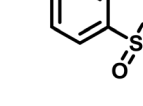
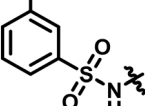
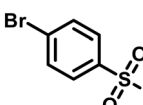
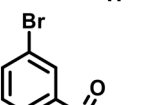
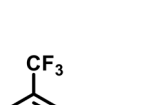
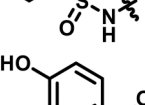
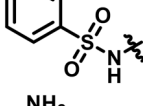
Intermediates **M11a–M11b** and compounds **K20–K22** were synthesized as depicted in Scheme 3. The synthetic effort

commenced with the Sonogashira coupling reaction between commercially available **M9a–M9b** and (triisopropylsilyl) acetylene to produce intermediates **M10a–M10b**, which were deprotected with tetrabutylammonium fluoride to obtain intermediates **M11a–M11b**. For target compounds **K20–K21**, intermediate **M2** underwent the Sonogashira coupling reaction with intermediates **M11a–M11b** to obtain key intermediate **M12a–M12b**. Intermediates **M13a–M13b** were obtained by the Goldberg-amination reaction between intermediates **M12a–M12b** and 4-nitrobenzenesulfonamide. Subsequently, intermediates **M13a–M13b** were reduced with iron powder under acidic conditions to obtain intermediates **M14a–M14b**, which were deprotected to yield compounds



**Fig. 3** (A) Binding mode of **K01** in the ATP-binding site of PLK4 (PDB code: 4JXF, colored green). (B) Binding mode of **K01** in the ATP-binding site of PLK4 (PDB code: 4JXF, surface mode). Interactions are illustrated with yellow or blue dashed lines. The ligands are depicted by element with carbons in yellow.

Table 1 *In vitro* PLK4 inhibition activity of K01 to K19

Entry	R <sub>1</sub>	PLK4 IC <sub>50</sub> (nM)	Entry	R <sub>1</sub>	PLK4 IC <sub>50</sub> (nM)
 K01-K19					
K01		977.6	K08		67.7
K02		12.4	K09		318.2
K03		103.1	K10		501.3
K04		240.6	K11		180.6
K05		184.3	K12		11.9
K06		67.5	K13		21.3
K07		23.6	K14		10.5
K15		818.2	K18		4.1
K16		19.5	K19		240.6
K17		0.3	Centrinone		2.7

**K20–K21.** **M2** underwent a Heck reaction with 3-vinylpyridine to obtain **M15**, and then *via* the same reaction conditions as **K20–K21** to obtain compound **K22**.

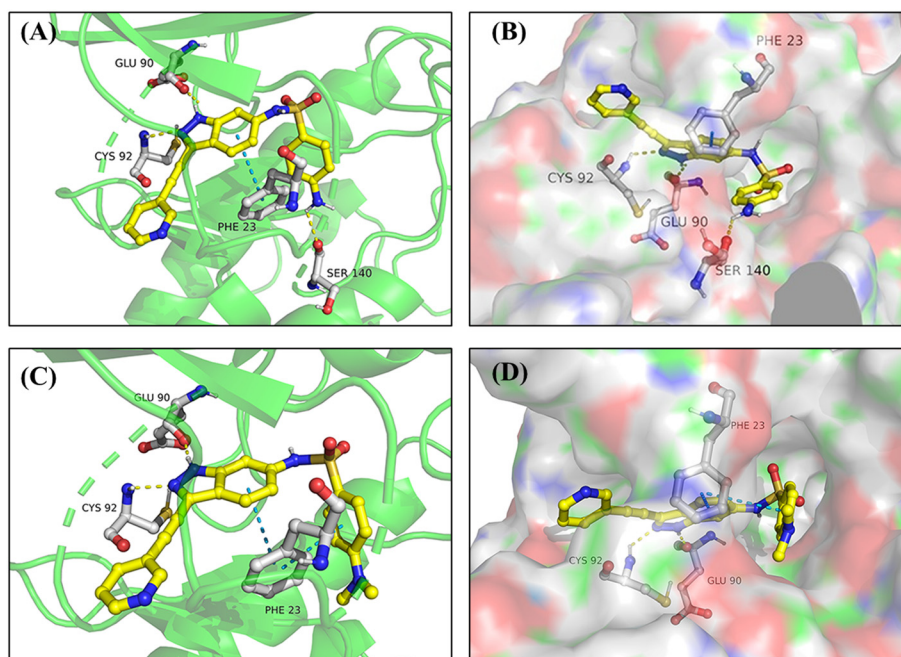
## 2.2 Target compound design and *in vitro* activity against PLK4 kinase

In order to assess the inhibitory activity of the newly synthesized compounds on PLK4 enzyme, we conducted *in vitro* testing using the LanthaScreen Eu kinase binding assay from Thermo Fisher Scientific in Carlsbad, USA. As a benchmark, **centrinone** was utilized as a positive control in our study. Remarkably, **centrinone** exhibited potent inhibition of PLK4 with an  $IC_{50}$  value of 2.7 nM under the specific experimental conditions we employed, aligning closely with data reported in previous studies.<sup>22</sup>

Initially, we confirmed the binding mechanism of compound **K01** with PLK4 (PDB code 4JXF) using molecular docking analysis. As predicted in our design, the indazole core of compound **K01** maintained hydrogen bond connections with the hinge area amino acid residues numbered as Glu-90 and Cys-92, while the 3-alkynylpyridine moiety extended into the solvent region, and the phenylsulfonamide fragment effectively occupied the hydrophobic cavity, which is essential for augmenting the inhibitor's efficacy,<sup>28</sup> with the benzene ring engaging in  $\pi$ - $\pi$  interactions with Phe-23 (Fig. 3A and B).

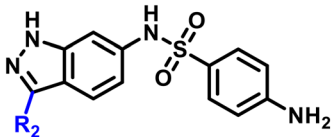
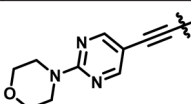
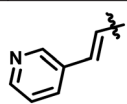
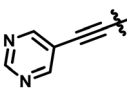
Guided by the docking study, we plan to include several substituents on the benzene ring to further investigate the structure–activity relationship of the hydrophobic cavity and

enhance the inhibitory efficacy against PLK4 (Table 1). Initially, we produced compounds **K02–K10** by including substituents at the *para*-position of the benzene ring. The kinase assay results indicate that compound **K02** ( $IC_{50}$  = 12.4 nM), including a methyl substituent, exhibited the highest activity among the alkyl substituents. Furthermore, as the substituent volume grew, the activity of compounds markedly diminished. In halogen-substituted groups, a rise in the atomic volume of halogen atoms correlates with a gradual enhancement in the reactivity of the compounds. Compound **K07**, with a bromine atom substitution, demonstrated excellent activity ( $IC_{50}$  = 23.6 nM). Nonetheless, the introduction of a bulky iodine atom resulted in a marked reduction of inhibitory activity. The activity of the *para*-trifluoromethoxy and *para*-methoxy molecules exhibited a notable decline. The aforementioned results demonstrate that the volume of this cavity section is finite. We subsequently included methyl groups, halogen atoms, and bulky groups at the *meta*-position of the benzene ring to create compounds **K11–K15**. *In vitro* kinase inhibition experiments revealed that compounds with halogen atom replacements at the *meta*-position exhibited higher activity compared to those with *para*-position substitutions, whereas the incorporation of bulky groups at the *meta*-position markedly diminished the activity. However, the PLK4 inhibitory activity was still not significantly enhanced. According to our previous research, the additional interaction between the inhibitors and the amino acid residue Lys-41 or Ser-140 in the hydrophobic cavity near the DFG motif has the potential to enhance the inhibitor activities of the



**Fig. 4** (A) Binding mode of **K17** in the ATP-binding site of PLK4 (PDB code: 4JXF, colored green). (B) Binding mode of **K17** in the ATP-binding site of PLK4 (PDB code: 4JXF, surface mode). (C) Binding mode of **K19** in the ATP-binding site of PLK4 (PDB code: 4JXF, colored green). (D) Binding mode of **K19** in the ATP-binding site of PLK4 (PDB code: 4JXF, surface mode). Interactions are illustrated with yellow or blue dashed lines. The ligands are depicted by element with carbons in yellow.

Table 2 *In vitro* PLK4 inhibition activity of K20 to K22

 K20-K22					
Entry	R <sub>2</sub>	PLK4 IC <sub>50</sub> (nM)	Entry	R <sub>2</sub>	PLK4 IC <sub>50</sub> (nM)
K20		15.6	K22		0.1
K21		184.3	Centrinone		2.7

inhibitors.<sup>29</sup> We endeavored to incorporate appropriate groups to engage with the adjacent amino acids; compounds **K16–K18** were created by integrating hydrogen bond donors onto the benzene ring. The results aligned with expectations, revealing that compound **K17**, including a *para*-amino alteration, demonstrated the most potent activity (PLK4 IC<sub>50</sub> = 0.3 nM).

The docking analysis of compound **K17** demonstrated that it preserved the initial hydrogen bonding contacts, moreover, the 4-amino group established a novel pair of hydrogen bonds with Ser-140, potentially accounting for the observed inhibition in activity enhancement (Fig. 4A and B). Consequently, to ascertain the role of hydrogen bond interactions in the activity, **K19** was produced. The activity of **K19** was significantly diminished, corroborating our theory and underscoring the significance of hydrogen bonding with Ser-140 (Fig. 4C and D).

Besides the hydrophobic pocket near the DFG motif, which has an important influence on the activity, the fragment extending towards the solvent region also has an effect on the activity. This segment can be modified to provide analogues with unique characteristics regarding isoform stability and cellular activity. Consequently, we

sought to enhance its hydrophilic components to further augment its activity and stability. We conducted exploration in the solvent zone based on compound **K17**. Compounds **K20–K22** were synthesized. Table 2 indicates that compounds **K20–K21** demonstrated a reduction in activity. Compound **K22** has shown better performance after a 3-ethenylpyridine was added. Molecular docking experiments indicate that compound **K22** preserves its initial hydrogen bond connections. The increased activity of **K22** may be due to the fact that the vinyl group, as opposed to an alkyne, may create a specific angle that could show a better binding mode with the protein (Fig. 5A and B).

### 2.3 Antiproliferative activity

In this study, compounds **K17**, **K18** and **K22** were selected for antiproliferation experiments on breast cancer cells (MCF-7).<sup>30</sup> **Centrinone** was used as a positive control (Table 3). The anti-proliferation ability of compound **K22** (IC<sub>50</sub> = 1.3 μM) was better than **centrinone** (IC<sub>50</sub> = 4.8 μM), and its selectivity coefficient for normal cell lines and the MCF-7 cell line was also better than that of **centrinone**.

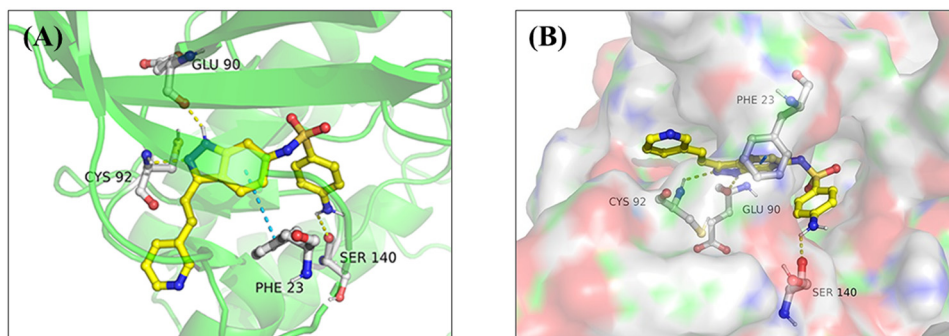
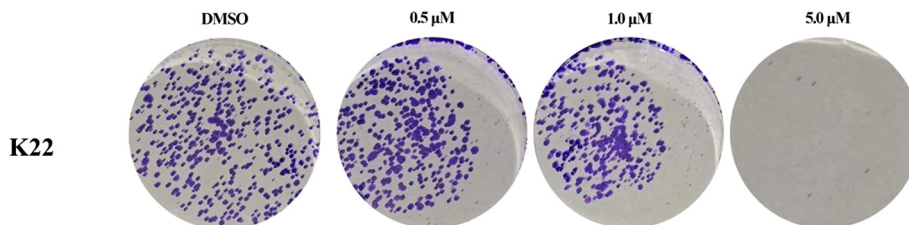


Fig. 5 (A) Binding mode of **K22** in the ATP-binding site of PLK4 (PDB code: 4JXF, colored green). (B) Binding mode of **K22** in the ATP-binding site of PLK4 (PDB code: 4JXF, surface mode). Interactions are illustrated with yellow or blue dashed lines. The ligands are depicted by element with carbons in yellow.

**Table 3** Antiproliferative activity (IC<sub>50</sub>, μM) of select compounds against MCF-7 and HEK293T cells

Compound	MCF-7 (μM)	HEK293T (μM)	SF (HEK293T/MCF-7) <sup>a</sup>
K17	16.6	9.1	0.5
K18	27.1	1.4	0.05
K22	1.3	3.1	2.3
Centrinone	4.8	0.9	0.19

<sup>a</sup> SF (HEK293T/MCF-7): selectivity factor for MCF-7 cells over HEK293T cells (SF(HEK293T/MCF-7) = IC<sub>50</sub>(HEK293T)/IC<sub>50</sub>(MCF-7)).

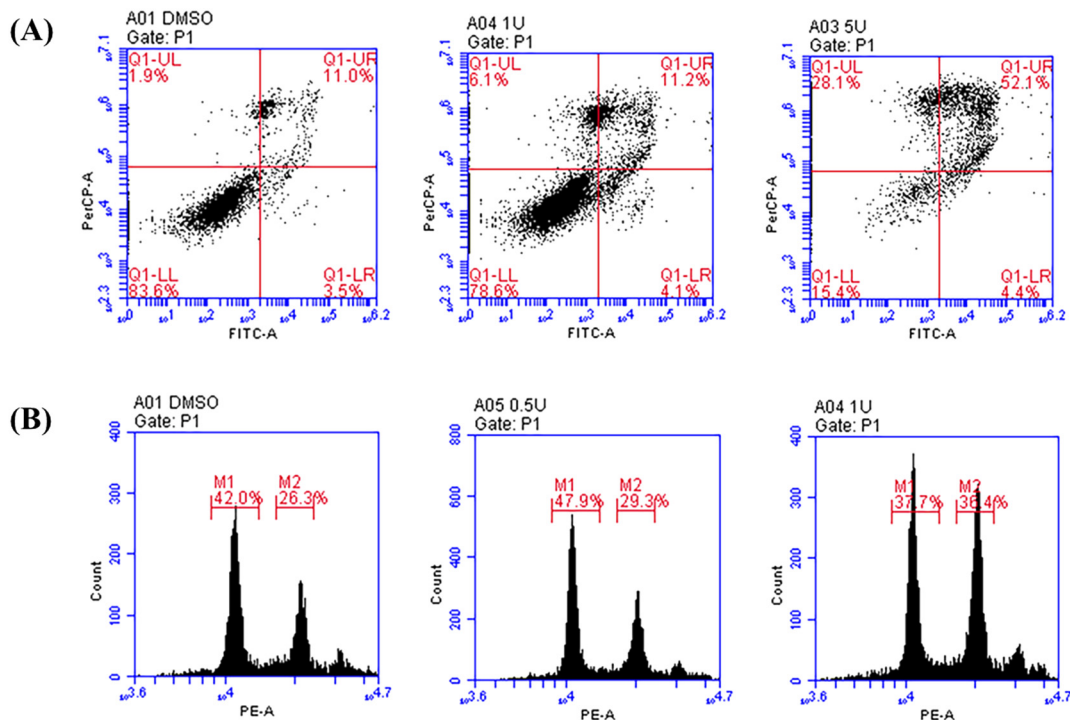
**Fig. 6** Clonogenic assay of MCF-7 cells treated with DMSO, K22.

#### 2.4 Effects of compound K22 on colony formation

The colony formation assay of MCF-7 cells treated with the PLK4 inhibitor K22 is shown in Fig. 6. Compound K22 demonstrates a concentration-dependent capacity to impede MCF-7 cell growth, and K22 has an acceptable ability to inhibit MCF-7 cell colon formation at 5 μM.

#### 2.5 Flow cytometry (MCF-7 cell apoptosis, cell cycle arrest) study

We employed flow cytometry to investigate the mechanism by which the inhibitor K22 exerts its anti-proliferative effect on MCF-7 cells, specifically assessing its capacity to induce apoptosis and cell cycle arrest. Fig. 7A demonstrates that the inhibitor K22 can induce apoptosis in MCF-7 cells in a

**Fig. 7** (A) K22 could induce cell apoptosis in MCF-7 cells. (B) K22 could induce cell cycle arrest in MCF-7 cells.

**Table 4** Liver microsomal stability of compound **K22**

Compound	Parameters	$k$ (1 min <sup>-1</sup> )	$T_{1/2}$ (min)	$CL_{int,microsome}$ ( $\mu\text{L min}^{-1} \text{mg}^{-1}$ proteins)	$CL_{int,in vivo}$ ( $\text{mL min}^{-1} \text{kg}^{-1}$ )
<b>K22</b>	Human	0.0136	51.0	27.2	25.7
	Rat	0.0467	14.8	93.4	168
	Mouse	0.0739	9.38	148	582

**Table 5** Binding rate of plasma protein of compound **K22**

Compound	Human				SD rat				ICR mouse			
	$f_u$	$f_b\%$	Recovery%	Stability%	$f_u\%$	$f_b\%$	Recovery%	Stability%	$f_u\%$	$f_b\%$	Recovery%	Stability%
<b>K22</b>	0.319	99.7	105	108	1.17	98.8	86.8	98.7	1.83	98.2	91.3	106

concentration-dependent manner, and the apoptotic rates were 15.3% and 56.5% at concentrations of 1.0 and 5.0  $\mu\text{M}$ , respectively. With the increasing concentration of compound **K22**, the apoptosis rate of MCF-7 cells progressively rises, the proportion of cells in the G2 phase escalates, and the proportion of cells in the G1 phase diminishes (Fig. 7B). These results indicated that **K22** could regulate G2/M centrosome replication by inhibiting PLK4, and thus arrested MCF-7 cell division (36.4%, G2/M phase at 1.0  $\mu\text{M}$ ).

### 2.6 *In vitro* binding rate of plasma protein and liver microsomal stability of compound **K22**

The *in vitro* metabolic stability of a compound is the foundation for exerting and maintaining its efficacy, and it is also one of the important factors to consider when evaluating druggability.<sup>31</sup> Consequently, we performed an *in vitro* liver microsome stability assay on compound **K22**, with the findings presented in Table 4. The *in vitro* liver microsomal stability assay showed that compound **K22** possessed good stability in human liver microsomal ( $T_{1/2} = 51.0$  min). Through the results of plasma protein binding experiments (Table 5), it is known that compound **K22** has an excellent plasma protein binding rate (human:  $f_b\% = 99.7\%$ ). The above experimental results indicate that compound **K22** is metabolically cleared at a slower rate, and it can produce a sustained effect.

### 2.7 ADME study of compound **K22**

Based on the above acceptable characteristics *in vitro*, the *in vivo* ADME properties of compound **K22** were further evaluated. After single intravenous (1 mg  $\text{kg}^{-1}$ ) administration, compound **K22** exhibited a good area under the curve ( $AUC_{0-t} = 447 \pm 47.6$  ng h  $\text{mL}^{-1}$ ,  $AUC_{0-inf} = 445 \pm 40.7$  ng h  $\text{mL}^{-1}$ ), acceptable half-life ( $T_{1/2} = 1.07 \pm 0.111$  h), acceptable residence time *in vivo* ( $MRT_{0-t} = 1.02 \pm 0.212$  h,

$MRT_{0-inf} = 1.11 \pm 0.128$  h). Summing up, compound **K22** exhibited acceptable pharmacokinetic properties (Table 6).

## 3. Conclusions

In this study, we conducted molecular docking research using **axitinib**, **CFI-400945** and **YLT-11**, and made a bunch of novel *N*-(1*H*-indazol-6-yl)benzenesulfonamide derivatives by using methods of structural simplification and fragment growth. The *in vitro* enzyme activity assays suggested that compound **K22** exhibited excellent inhibitory activity against PLK4 (PLK4  $IC_{50} = 0.1$  nM). In the antiproliferation experiments, compound **K22** ( $IC_{50} = 1.3$   $\mu\text{M}$ ) had greater inhibitory efficacy against the MCF-7 breast cancer cell line than **centrinone** ( $IC_{50} = 4.8$   $\mu\text{M}$ ). Compound **K22** strongly inhibited colony formation in MCF-7 cells at 5  $\mu\text{M}$ . Compound **K22** could induce apoptosis, and it could regulate G2/M centrosome replication by inhibiting PLK4, and thus arrest MCF-7 cell division. Remarkably, **K22** showed acceptable human liver microsome stability ( $T_{1/2} = 51.0$  min), and it has an excellent plasma protein binding rate. The pharmacokinetic study showed that compound **K22** exhibited a good area under the curve ( $AUC_{0-t} = 447 \pm 47.6$  ng h  $\text{mL}^{-1}$ ) and acceptable half-life ( $T_{1/2} = 1.07 \pm 0.111$  h). In conclusion, compound **K22** is an excellent PLK4 inhibitor and has further research value as a lead compound.

**Table 6** ADME profiles of compound **K22**

PK parameters	<b>K22</b>	
	<i>i.v.</i> 1 mg $\text{kg}^{-1}$	
	Mean	SD
$AUC_{0-t}$ (ng h $\text{mL}^{-1}$ )	447	47.6
$AUC_{0-inf}$ (ng h $\text{mL}^{-1}$ )	445	40.7
$T_{1/2}$ (h)	1.07	0.111
CL ( $\text{mg kg}^{-1} \text{min}^{-1}$ )	36.9	3.23
Vdss	2.44	0.164
$MRT_{0-t}$ (h)	1.02	0.212
$MRT_{0-inf}$ (h)	1.11	0.128

## 4. Experiments

Unless stated otherwise, the reagents and solvents utilized in this experiment are commercially acquired and can be employed immediately without purification. The production and storage of anhydrous reagents are conducted in accordance with established protocols. Reactions that are sensitive to moisture and oxygen are performed in a dry argon environment utilizing anhydrous vessels and solvents. Thin-layer chromatography utilizing fluorescent F-254 silica gel plates is employed to observe the reactions. Column chromatography purification is conducted utilizing silica gel (200–300 mesh ASTM). All target chemicals were examined using nuclear magnetic resonance (NMR), high-resolution mass spectrometry (HRMS) and melting point analysis. NMR data were acquired in DMSO-*d*<sub>6</sub> using Bruker ARX-600 NMR spectrometers, employing TMS as an internal standard. High-resolution mass spectrometry (HRMS) for all target substances was conducted using a Q-TOF Bruker mass spectrometer with an electrospray ionization (ESI) detector. Melting points were determined on the BüCHI melting point B-540 melting point apparatus.

### 4.1 Chemistry

**General procedure for synthesis of intermediate M1.** To a stirring solution of 6-bromoindazole (5.00 g, 25.37 mmol, 1.0 equiv.) in anhydrous DMF (30 mL), NIS (8.56 g, 38.07 mmol, 1.5 equiv.) was added at room temperature and the mixture was stirred for 5 h. The reaction was monitored by TLC. The mixture was poured into water to precipitate, filtered, washed, and dried. Brown solid (7.09 g), yield 86.5%.

**General procedure for synthesis of compound M2.** To a solution of M1 (4.00 g, 12.38 mmol, 1.0 equiv.) and *p*-toluenesulfonic acid (213.5 mg, 1.24 mmol, 0.1 equiv.) in anhydrous DCM (20 mL) was incrementally introduced the DCM solution of DHP (1.56 g, 18.58 mmol, 1.5 equiv.) at 0 °C. Upon completion of the addition, the reaction was stirred at room temperature for 4 h. The reaction progress was monitored by TLC. Quenching reaction used saturated sodium bicarbonate, followed by DCM extraction. The residue was purified using silica chromatography. White solid (4.44 g), yield 88.1%.

**General procedure for synthesis of compound M3.** 3-Alkynylpyridine (608.01 mg, 5.90 mmol, 1.2 equiv.) was added to a solution of M2 (2.00 g, 4.91 mmol, 1.0 equiv.) in TEA (30 mL). The mixture was degassed with argon for 3 minutes, then add CuI (18.7 mg, 0.098 mmol, 0.02 equiv.) and Pd(PPh<sub>3</sub>)<sub>4</sub> (56.6 mg, 0.049 mmol, 0.01 equiv.), and the mixture was stirred at room temperature for 4 h. The reaction was monitored by TLC. A saturated ammonium chloride solution was used to quench the reaction, followed by ethyl acetate extraction. The organic solvent removed under reduced pressure, and the residue was refined using silica chromatography. White solid (1.57 g), yield 83.4%.

**General procedure for synthesis of intermediates M4a–M4i.** To a solution of M3 (150.00 mg, 0.39 mmol, 1.0

equiv.) in dry acetonitrile (2 mL), toluenesulfonamide (80.18 mg, 0.51 mmol, 1.3 equiv.) or its derivatives and K<sub>2</sub>CO<sub>3</sub> (161.71 mg, 1.17 mmol, 3.0 equiv.) were added, followed by degasification with argon for 3 min. Subsequently, CuI (37.14 mg, 0.20 mmol, 0.5 equiv.) and DMEDA (34.52 mg, 0.39 mmol, 1.0 equiv.) were added. The mixture was stirred in a sealed tube at 100 °C for 12 h. The reaction was monitored by TLC. The mixture was filtered through a pad of Celite, and the residue was purified using silica chromatography. White solid (125.36 mg), yield 59.7–70.1%.

**General procedure for synthesis of compound K01.** A mixture of M4a (100.00 mg, 0.22 mmol, 1.0 equiv.) and *p*-toluenesulfonic acid (563.31 mg, 3.27 mmol, 15.0 equiv.) in MeOH (3 mL) and H<sub>2</sub>O (1 mL) was stirred at 80 °C for 3 h. The reaction was monitored by TLC. Adjust the pH to 7 with saturated sodium bicarbonate solution, followed by ethyl acetate extraction. The organic solvent was removed under reduced pressure, and the residue was purified using silica chromatography. White solid (56.26 mg), yield 68.3%.

**General procedure for synthesis of compounds K02–K03, K06–K07, K09, K14–K15, K18.** The synthesis method of K02–K03, K06–K07, K09, K14–K15, K18 was similar to K01.

*N*-(3-(Pyridin-3-ylethynyl)-1H-indazol-6-yl)benzenesulfonamide (K01). White solid, yield 68.3%, m.p. 229.5–230.4 °C. <sup>1</sup>H NMR (600 MHz, DMSO-*d*<sub>6</sub>) δ 13.38 (s, 1H), 10.57 (s, 1H), 8.83 (d, *J* = 2.0 Hz, 1H), 8.61 (dd, *J* = 4.8, 1.5 Hz, 1H), 8.05 (dt, *J* = 7.9, 1.8 Hz, 1H), 7.78 (d, *J* = 8.2 Hz, 2H), 7.73 (d, *J* = 8.7 Hz, 1H), 7.61–7.58 (m, 1H), 7.56–7.53 (m, 2H), 7.49 (dd, *J* = 7.8, 4.9 Hz, 1H), 7.32 (s, 1H), 7.03 (d, *J* = 8.7 Hz, 1H). <sup>13</sup>C NMR (151 MHz, DMSO-*d*<sub>6</sub>) δ 152.13, 149.69, 140.82, 139.68, 139.11, 137.45, 133.54, 129.81 (2C), 127.73, 127.10 (2C), 124.15, 121.46, 121.04, 119.50, 116.57, 100.79, 89.70, 84.88. HRMS (ESI, *m/z*) calcd for C<sub>20</sub>H<sub>14</sub>N<sub>4</sub>NaO<sub>2</sub>S [M + Na]<sup>+</sup>: 397.0730; found: 397.0754.

4-Methyl-*N*-(3-(pyridin-3-ylethynyl)-1H-indazol-6-yl)benzenesulfonamide (K02). White solid (54.44 mg), yield 63.7%, m.p. 238.1–239.0 °C <sup>1</sup>H NMR (600 MHz, DMSO-*d*<sub>6</sub>) δ 13.37 (s, 1H), 10.50 (s, 1H), 8.84 (d, *J* = 1.4 Hz, 1H), 8.62 (dd, *J* = 4.8, 1.6 Hz, 1H), 8.07–8.05 (m, 1H), 7.73 (d, *J* = 8.7 Hz, 1H), 7.67 (d, *J* = 8.3 Hz, 2H), 7.50 (dd, *J* = 7.5, 4.5 Hz, 1H), 7.34 (d, *J* = 8.1 Hz, 2H), 7.31 (d, *J* = 1.2 Hz, 1H), 7.03 (dd, *J* = 8.7, 1.7 Hz, 1H), 2.31 (s, 3H). <sup>13</sup>C NMR (151 MHz, DMSO-*d*<sub>6</sub>) δ 152.15, 149.70, 143.92, 140.84, 139.10, 137.60, 136.85, 130.23 (2C), 127.71, 127.17 (2C), 124.14, 121.39, 121.00, 119.51, 116.44, 100.53, 89.68, 84.92, 21.41. HRMS (ESI, *m/z*) calcd for C<sub>21</sub>H<sub>16</sub>N<sub>4</sub>NaO<sub>2</sub>S [M + Na]<sup>+</sup>: 411.0994; found: 411.0917.

4-Ethyl-*N*-(3-(pyridin-3-ylethynyl)-1H-indazol-6-yl)benzenesulfonamide (K03). White solid (53.83 mg), yield 60.8%, m.p. 222.5–223.7 °C. <sup>1</sup>H NMR (600 MHz, DMSO-*d*<sub>6</sub>) δ 13.37 (s, 1H), 10.52 (s, 1H), 8.83 (d, *J* = 1.6 Hz, 1H), 8.61 (dd, *J* = 4.8, 1.4 Hz, 1H), 8.05 (dt, *J* = 7.9, 1.7 Hz, 1H), 7.73 (d, *J* = 8.7 Hz, 1H), 7.69 (d, *J* = 8.3 Hz, 2H), 7.49 (dd, *J* = 7.8, 4.9 Hz, 1H), 7.37 (d, *J* = 8.3 Hz, 2H), 7.32 (s, 1H), 7.03 (dd, *J* = 8.7, 1.5 Hz, 1H), 2.61 (q, *J* = 7.6 Hz, 2H), 1.12 (t, *J* = 7.6 Hz, 3H). <sup>13</sup>C NMR (151 MHz, DMSO-*d*<sub>6</sub>) δ 152.15, 149.83, 149.70, 140.85, 139.10, 137.61, 137.15, 129.10 (2C), 127.71, 127.24 (2C),

124.14, 121.35, 121.02, 119.51, 116.35, 100.38, 89.67, 84.92, 28.38, 15.34. HRMS (ESI,  $m/z$ ) calcd for  $C_{22}H_{18}N_4NaO_2S$  [ $M + Na$ ]<sup>+</sup>: 425.1043; found: 425.1075.

*4-Chloro-N-(3-(pyridin-3-ylethynyl)-1H-indazol-6-yl)*

*benzenesulfonamide (K06)*. White solid (53.43 mg), yield 59.4%, m.p. 232.5–233.1 °C. <sup>1</sup>H NMR (600 MHz, DMSO-*d*<sub>6</sub>) δ 13.42 (s, 1H), 10.63 (s, 1H), 8.84 (d,  $J = 1.4$  Hz, 1H), 8.62 (dd,  $J = 4.8, 1.6$  Hz, 1H), 8.06 (dt,  $J = 7.9, 1.9$  Hz, 1H), 7.77–7.75 (m, 3H), 7.63 (d,  $J = 8.7$  Hz, 2H), 7.50 (dd,  $J = 7.9, 4.9$  Hz, 1H), 7.32 (d,  $J = 1.1$  Hz, 1H), 7.02 (dd,  $J = 8.7, 1.7$  Hz, 1H). <sup>13</sup>C NMR (151 MHz, DMSO-*d*<sub>6</sub>) δ 152.16, 149.70, 140.79, 139.10, 138.51, 138.44, 137.09, 129.99 (2C), 129.05 (2C), 127.77, 124.13, 121.69, 121.15, 119.49, 116.74, 101.35, 89.74, 84.86. HRMS (ESI,  $m/z$ ) calcd for  $C_{20}H_{14}ClN_4O_2S$  [ $M + H$ ]<sup>+</sup>: 409.0521; found: 409.0550.

*4-Bromo-N-(3-(pyridin-3-ylethynyl)-1H-indazol-6-yl)*

*benzenesulfonamide (K07)*. White solid (51.46 mg), yield 51.6%, m.p. 208.1–209.7 °C. <sup>1</sup>H NMR (600 MHz, DMSO-*d*<sub>6</sub>) δ 13.41 (s, 1H), 10.62 (s, 1H), 8.84 (s, 1H), 8.62 (s, 1H), 8.00 (d,  $J = 73.0$  Hz, 1H), 7.79–7.46 (m, 6H), 7.31 (s, 1H), 7.02 (s, 1H). <sup>13</sup>C NMR (151 MHz, DMSO-*d*<sub>6</sub>) δ 152.15, 149.69, 140.79, 139.26, 139.15, 138.72 (2C), 137.11, 128.96 (2C), 127.77, 124.17, 121.62, 121.16, 119.49, 116.68, 101.88, 101.19, 89.74, 84.85. HRMS (ESI,  $m/z$ ) calcd for  $C_{20}H_{14}BrN_4O_2S$  [ $M + H$ ]<sup>+</sup>: 453.0015; found: 453.0039.

*4-Methoxy-N-(3-(pyridin-3-ylethynyl)-1H-indazol-6-yl)*

*benzenesulfonamide (K09)*. White solid (53.56 mg), yield 60.2%, m.p. 121.0–121.8 °C. <sup>1</sup>H NMR (600 MHz, DMSO-*d*<sub>6</sub>) δ 13.37 (s, 1H), 10.42 (s, 1H), 8.83 (s, 1H), 8.61 (d,  $J = 3.4$  Hz, 1H), 8.06 (d,  $J = 7.5$  Hz, 1H), 7.73 (s, 1H), 7.70 (d,  $J = 8.6$  Hz, 2H), 7.50 (d,  $J = 4.9$  Hz, 1H), 7.31 (s, 1H), 7.05 (d,  $J = 8.7$  Hz, 2H), 7.02 (s, 1H), 3.77 (s, 3H). <sup>13</sup>C NMR (151 MHz, DMSO-*d*<sub>6</sub>) δ 162.98, 152.06, 149.62, 140.88, 139.19, 137.70, 131.25, 129.36 (2C), 127.69, 124.20, 121.35, 120.98, 119.55, 116.50, 114.91 (2C), 100.52, 89.67, 84.94, 56.07. HRMS (ESI,  $m/z$ ) calcd for  $C_{21}H_{16}N_4NaO_3S$  [ $M + Na$ ]<sup>+</sup>: 427.0835; found: 427.0866.

*3-Bromo-N-(3-(pyridin-3-ylethynyl)-1H-indazol-6-yl)*

*benzenesulfonamide (K14)*. White solid (57.14 mg), yield 57.3%, m.p. 215.0–215.8 °C. <sup>1</sup>H NMR (600 MHz, DMSO-*d*<sub>6</sub>) δ 13.42 (s, 1H), 10.62 (s, 1H), 8.84 (s, 1H), 8.62 (s, 1H), 8.08 (d,  $J = 16.7$  Hz, 1H), 7.84–7.72 (m, 3H), 7.63–7.47 (m, 3H), 7.32 (s, 1H), 7.03 (d,  $J = 7.6$  Hz, 1H). HRMS (ESI,  $m/z$ ) calcd for  $C_{20}H_{12}BrN_4O_2S$  [ $M - H$ ]<sup>-</sup>: 450.9923; found: 450.9922.

*N-(3-(Pyridin-3-ylethynyl)-1H-indazol-6-yl)-3-(trifluoromethyl)*

*benzenesulfonamide (K15)*. White solid (44.97 mg), yield 46.2%, m.p. 134.7–135.4 °C. <sup>1</sup>H NMR (600 MHz, DMSO-*d*<sub>6</sub>) δ 13.43 (s, 1H), 10.71 (s, 1H), 8.84 (d,  $J = 1.4$  Hz, 1H), 8.61 (d,  $J = 4.7$  Hz, 1H), 8.06 (d,  $J = 7.8$  Hz, 2H), 8.01 (s, 2H), 7.80 (d,  $J = 7.9$  Hz, 1H), 7.77 (d,  $J = 8.5$  Hz, 1H), 7.50–7.47 (m, 1H), 7.34 (s, 1H), 7.02 (d,  $J = 8.6$  Hz, 1H). <sup>13</sup>C NMR (151 MHz, DMSO) δ 152.12, 149.70, 140.72 (d,  $J = 4.4$  Hz), 139.13, 136.76, 131.52, 131.16, 130.35 (q,  $J = 32.7$  Hz), 130.31 (d,  $J = 2.9$  Hz), 127.79, 124.15, 123.71 (q,  $J = 272.8$  Hz), 123.63 (d,  $J = 3.7$  Hz), 123.60, 121.82, 121.26, 119.46, 116.91, 101.81, 89.77, 84.76. HRMS (ESI,  $m/z$ ) calcd for  $C_{21}H_{14}F_3N_4O_2S$  [ $M + H$ ]<sup>+</sup>: 443.0821; found: 443.0822.

*4-Hydroxy-N-(3-(pyridin-3-ylethynyl)-1H-indazol-6-yl)*

*benzenesulfonamide (K18)*. White solid, (44.32 mg) yield 51.6%, m.p. 260.5–261.4 °C. <sup>1</sup>H NMR (600 MHz, DMSO-*d*<sub>6</sub>) δ 13.67 (s, 1H), 8.87 (s, 1H), 8.64 (d,  $J = 2.8$  Hz, 1H), 8.39 (d,  $J = 8.7$  Hz, 2H), 8.09 (d,  $J = 7.9$  Hz, 1H), 7.85 (d,  $J = 8.6$  Hz, 1H), 7.79 (d,  $J = 8.7$  Hz, 2H), 7.51 (dd,  $J = 7.6, 5.0$  Hz, 1H), 7.40 (s, 1H), 6.98 (dd,  $J = 8.7, 1.3$  Hz, 1H). <sup>13</sup>C NMR (151 MHz, DMSO-*d*<sub>6</sub>) δ 161.85, 151.73, 149.20, 140.91, 139.66, 137.88, 129.58, 129.56, 128.53, 127.60, 125.97, 124.36, 121.28, 120.89, 119.73, 116.49, 116.09, 100.38, 89.49, 85.20. HRMS (ESI,  $m/z$ ) calcd for  $C_{20}H_{14}N_4NaO_3S$  [ $M + Na$ ]<sup>+</sup>: 413.0701; found: 413.0710. Retention time 3.269 min, HPLC purity = 99.26%.

**General procedure for synthesis of compound M5.** The solution of starting material **M3** (1.00 g, 2.62 mmol, 1.0 equiv.), *tert*-butyl carbamate (499.7 mg, 3.92 mmol, 1.5 equiv.) and  $Cs_2CO_3$  (2.56 g, 7.86 mmol, 3.0 equiv.) in anhydrous 1,4-dioxane (6 mL) was degassed with argon for 3 min.  $Pd_2(dba)_3$  (24.00 mg, 0.026 mmol, 0.01 equiv.) and xantphos (30.32 mg, 0.052 mmol, 0.02 equiv.) were added, and the mixture was stirred at 100 °C for 4 h. The reaction was monitored by TLC. The organic solvent removed under reduced pressure, and the residue was refined using silica chromatography. White solid (848.67 mg), yield 77.4%.

**General procedure for synthesis of compound M6.** The synthesis method of **M6** was similar to **K01**. Pale yellow solid (187.24 mg), yield 66.9%.

**General procedure for synthesis of compound K04–K05, K08, K10–K13, K19.** A mixture of **M6** (50 mg, 0.21 mmol, 1.0 equiv.), DMAP (2.56 mg, 0.21 mmol, 1.0 equiv.) and benzenyl chloride derivatives (0.25 mmol, 1.2 equiv.) in dry pyridine (5 mL) was stirred at room temperature for 3 h. The reaction was monitored by TLC. The organic solvent removed under reduced pressure, followed by ethyl acetate extraction. The residue was refined using silica chromatography to obtain compounds **K04–K05, K08, K10–K13, K19**.

*4-Isopropyl-N-(3-(pyridin-3-ylethynyl)-1H-indazol-6-yl)*

*benzenesulfonamide (K04)*. White solid (49.94 mg), yield 57.1%, m.p. 211.5–212.3 °C. <sup>1</sup>H NMR (600 MHz, DMSO-*d*<sub>6</sub>) δ 13.38 (s, 1H), 10.56 (s, 1H), 8.83 (d,  $J = 1.5$  Hz, 1H), 8.61 (dd,  $J = 4.8, 1.5$  Hz, 1H), 8.05 (dt,  $J = 7.9, 1.8$  Hz, 1H), 7.74 (d,  $J = 8.8$  Hz, 1H), 7.72 (d,  $J = 8.4$  Hz, 2H), 7.48 (dd,  $J = 7.5, 4.9$  Hz, 1H), 7.41 (d,  $J = 8.4$  Hz, 2H), 7.35 (d,  $J = 1.1$  Hz, 1H), 7.05 (dd,  $J = 8.7, 1.7$  Hz, 1H), 2.93–2.87 (m, 1H), 1.14 (d,  $J = 6.9$  Hz, 6H). <sup>13</sup>C NMR (151 MHz, DMSO-*d*<sub>6</sub>) δ 154.29, 152.15, 149.69, 140.88, 139.09, 137.64, 137.37, 127.75, 127.72 (2C), 127.26 (2C), 124.14, 121.32, 121.04, 119.51, 116.24, 100.21, 89.67, 84.93, 33.76, 23.80 (2C). HRMS (ESI,  $m/z$ ) calcd for  $C_{23}H_{20}N_4NaO_2S$  [ $M + Na$ ]<sup>+</sup>: 439.1200; found: 439.1228.

*4-Fluoro-N-(3-(pyridin-3-ylethynyl)-1H-indazol-6-yl)*

*benzenesulfonamide (K05)*. White solid (46.81 mg), yield 56.8%, m.p. 238.1–239.0 °C. <sup>1</sup>H NMR (600 MHz, DMSO-*d*<sub>6</sub>) δ 13.40 (s, 1H), 10.57 (s, 1H), 8.83 (s, 1H), 8.62 (d,  $J = 4.7$  Hz, 1H), 8.06 (d,  $J = 7.9$  Hz, 1H), 7.85–7.80 (m, 2H), 7.75 (d,  $J = 8.7$  Hz, 1H), 7.49 (dd,  $J = 7.8, 4.9$  Hz, 1H), 7.41–7.37 (m, 2H), 7.31 (s, 1H), 7.01 (d,  $J = 8.7$  Hz, 1H). <sup>13</sup>C NMR (151 MHz, DMSO-*d*<sub>6</sub>) δ 164.84 (d,  $J = 251.4$  Hz), 152.10, 149.67, 140.80,

139.16, 137.22, 136.00 (d,  $J = 2.5$  Hz), 130.19 (2C, d,  $J = 9.9$  Hz), 127.75, 124.19, 121.61, 121.11, 119.51, 117.04 (2C, d,  $J = 23.0$  Hz), 116.73, 101.22, 89.72, 84.85.

**4-Iodo-N-(3-(pyridin-3-ylethynyl)-1H-indazol-6-yl)benzenesulfonamide (K08).** White solid (54.21 mg), yield 51.6%, m.p. 263.7–264.4 °C.  $^1\text{H}$  NMR (600 MHz, DMSO- $d_6$ )  $\delta$  13.40 (s, 1H), 10.61 (s, 1H), 8.83 (d,  $J = 2.1, 0.7$  Hz, 1H), 8.61 (dd,  $J = 4.8, 1.6$  Hz, 1H), 8.06 (dt,  $J = 7.9, 1.9$  Hz, 1H), 7.93 (d,  $J = 8.6$  Hz, 2H), 7.75 (d,  $J = 8.7$  Hz, 1H), 7.52–7.49 (m, 2H), 7.49–7.47 (m, 1H), 7.31 (d,  $J = 1.3$  Hz, 1H), 7.01 (dd,  $J = 8.7, 1.7$  Hz, 1H).  $^{13}\text{C}$  NMR (151 MHz, DMSO- $d_6$ )  $\delta$  152.12, 149.69, 140.79, 139.26, 139.15, 138.72 (2C), 137.11, 128.76 (2C), 127.77, 124.17, 121.62, 121.16, 119.49, 116.68, 101.88, 101.19, 89.74, 84.85. HRMS (ESI,  $m/z$ ) calcd for  $\text{C}_{20}\text{H}_{14}\text{IN}_4\text{O}_2\text{S}$  [ $\text{M} + \text{H}$ ] $^+$ : 500.9877; found: 500.9901.

**N-(3-(Pyridin-3-ylethynyl)-1H-indazol-6-yl)-4-(trifluoromethyl)benzenesulfonamide (K10).** White solid (48.78 mg), yield 52.5%, m.p. 197.5–198.2 °C.  $^1\text{H}$  NMR (600 MHz, DMSO- $d_6$ )  $\delta$  13.42 (s, 1H), 10.78 (s, 1H), 8.83 (d,  $J = 1.1$  Hz, 1H), 8.61 (dd,  $J = 4.7, 1.2$  Hz, 1H), 8.05 (dt,  $J = 7.9, 1.9$  Hz, 1H), 7.97–7.94 (m, 4H), 7.76 (d,  $J = 8.7$  Hz, 1H), 7.49 (dd,  $J = 7.6, 4.6$  Hz, 1H), 7.34 (d,  $J = 1.2$  Hz, 1H), 7.02 (dd,  $J = 8.7, 1.7$  Hz, 1H).  $^{13}\text{C}$  NMR (151 MHz, DMSO- $d_6$ )  $\delta$  152.13, 149.71, 143.56, 140.77, 139.12, 136.81, 133.14 (q,  $J = 32.4$  Hz), 128.11, 127.80 (2C), 127.11 (2C, d,  $J = 3.6$  Hz), 124.16, 123.77 (q,  $J = 273.0$  Hz), 121.78, 121.25, 119.47, 116.77, 101.57, 89.76, 84.79. HRMS (ESI,  $m/z$ ) calcd for  $\text{C}_{21}\text{H}_{13}\text{F}_3\text{N}_4\text{O}_2\text{S}$  [ $\text{M} + \text{H}$ ] $^+$ : 443.0800; found: 443.0801.

**3-Methyl-N-(3-(pyridin-3-ylethynyl)-1H-indazol-6-yl)benzenesulfonamide (K11).** White solid (45.93 mg), yield 56.3%, m.p. 255.7–256.5 °C.  $^1\text{H}$  NMR (600 MHz, DMSO- $d_6$ )  $\delta$  13.37 (s, 1H), 10.54 (s, 1H), 8.83 (d,  $J = 1.4$  Hz, 1H), 8.61 (dd,  $J = 4.8, 1.6$  Hz, 1H), 8.06 (dt,  $J = 7.9, 1.9$  Hz, 1H), 7.74 (d,  $J = 8.7$  Hz, 1H), 7.62 (s, 1H), 7.56 (d,  $J = 3.7$  Hz, 1H), 7.49 (dd,  $J = 7.9, 5.5$  Hz, 1H), 7.43–7.41 (m, 2H), 7.31 (d,  $J = 1.3$  Hz, 1H), 7.03 (dd,  $J = 8.7, 1.7$  Hz, 1H), 2.33 (s, 3H).  $^{13}\text{C}$  NMR (151 MHz, DMSO- $d_6$ )  $\delta$  152.15, 149.69, 140.84, 139.73, 139.52, 139.10, 137.52, 134.16, 129.64, 127.72, 127.31, 124.29, 124.14, 121.40, 121.02, 119.51, 116.43, 100.55, 89.68, 84.93, 21.29. HRMS (ESI,  $m/z$ ) calcd for  $\text{C}_{21}\text{H}_{16}\text{N}_4\text{NaO}_2\text{S}$  [ $\text{M} + \text{Na}$ ] $^+$ : 411.0911; found: 411.0921.

**3-Fluoro-N-(3-(pyridin-3-ylethynyl)-1H-indazol-6-yl)benzenesulfonamide (K12).** White solid (42.11 mg), yield 57.1%, m.p. 225.3.1–226.0 °C.  $^1\text{H}$  NMR (600 MHz, DMSO- $d_6$ )  $\delta$  13.40 (s, 1H), 10.67 (s, 1H), 8.84 (d,  $J = 1.4$  Hz, 1H), 8.62 (dd,  $J = 4.8, 1.6$  Hz, 1H), 8.06 (dt, 1H), 7.76 (d,  $J = 8.7$  Hz, 1H), 7.61–7.59 (m, 2H), 7.57 (d,  $J = 8.1$  Hz, 1H), 7.51–7.47 (m, 2H), 7.33 (d,  $J = 1.2$  Hz, 1H), 7.03 (dd,  $J = 8.7, 1.7$  Hz, 1H).  $^{13}\text{C}$  NMR (151 MHz, DMSO- $d_6$ )  $\delta$  162.09 (d,  $J = 248.7$  Hz), 152.14, 149.70, 141.67 (d,  $J = 6.5$  Hz), 140.78, 139.12, 136.99, 132.33, 127.78, 124.15, 123.46 (d,  $J = 2.3$  Hz), 121.69, 121.17, 120.74, 119.48, 116.72, 114.14 (d,  $J = 24.5$  Hz), 101.35, 89.75, 84.83. HRMS (ESI,  $m/z$ ) calcd for  $\text{C}_{20}\text{H}_{14}\text{FN}_4\text{O}_2\text{S}$  [ $\text{M} + \text{H}$ ] $^+$ : 393.0816; found: 393.0843.

**3-Chloro-N-(3-(pyridin-3-ylethynyl)-1H-indazol-6-yl)benzenesulfonamide (K13).** White solid (42.33 mg), yield

49.3%, m.p. 243.1–244.0 °C.  $^1\text{H}$  NMR (600 MHz, DMSO- $d_6$ )  $\delta$  13.41 (s, 1H), 10.67 (s, 1H), 8.84 (d,  $J = 1.4$  Hz, 1H), 8.62 (dd,  $J = 4.8, 1.6$  Hz, 1H), 8.06 (dt,  $J = 7.9, 1.9$  Hz, 1H), 7.79 (t,  $J = 1.9$  Hz, 1H), 7.77 (d,  $J = 8.7$  Hz, 1H), 7.71 (s, 1H), 7.69 (s, 1H), 7.58 (t,  $J = 8.0$  Hz, 1H), 7.49 (dd,  $J = 7.9, 4.9$  Hz, 1H), 7.32 (d,  $J = 1.5$  Hz, 1H), 7.03 (dd,  $J = 8.7, 1.6$  Hz, 1H).  $^{13}\text{C}$  NMR (151 MHz, DMSO- $d_6$ )  $\delta$  152.15, 149.71, 141.48, 140.77, 139.11, 136.94, 134.36, 133.58, 131.93, 127.79, 126.67, 125.87, 124.14, 121.72, 121.22, 119.48, 116.73, 101.40, 89.76, 84.83. HRMS (ESI,  $m/z$ ) calcd for  $\text{C}_{20}\text{H}_{14}\text{ClN}_4\text{O}_2\text{S}$  [ $\text{M} + \text{H}$ ] $^+$ : 409.0521; found: 409.0549.

**4-(Dimethylamino)-N-(3-(pyridin-3-ylethynyl)-1H-indazol-6-yl)benzenesulfonamide (K19).** White solid (38.75 mg), yield 44.2%, m.p. 214.5–215.2 °C.  $^1\text{H}$  NMR (600 MHz, DMSO- $d_6$ )  $\delta$  13.34 (s, 1H), 10.23 (s, 1H), 8.83 (d,  $J = 1.4$  Hz, 1H), 8.61 (dd,  $J = 4.8, 1.5$  Hz, 1H), 8.05 (dt,  $J = 7.9, 1.8$  Hz, 1H), 7.70 (d,  $J = 8.7$  Hz, 1H), 7.56 (s, 1H), 7.54 (s, 1H), 7.49 (dd,  $J = 7.8, 4.9$  Hz, 1H), 7.30 (s, 1H), 7.03 (dd,  $J = 8.7, 1.4$  Hz, 1H), 6.68 (d,  $J = 9.1$  Hz, 2H), 2.92 (s, 6H).  $^{13}\text{C}$  NMR (151 MHz, DMSO- $d_6$ )  $\delta$  153.06, 152.11, 149.66, 140.95, 139.12 (2C), 138.25, 128.86, 127.65, 124.52, 124.16, 121.06, 120.80, 119.54 (2C), 116.25, 111.26, 99.74, 89.61, 85.02, 39.98 (2C). HRMS (ESI,  $m/z$ ) calcd for  $\text{C}_{22}\text{H}_{19}\text{N}_5\text{NaO}_2\text{S}$  [ $\text{M} + \text{Na}$ ] $^+$ : 440.1152; found: 440.1177.

**General procedure for synthesis of intermediates M7a–M7b.** To a solution of 3-nitrophenylsulfonamide or 4-nitrophenylsulfonamide (102.51 mg, 0.51 mmol, 1.3 equiv.), **M3** (150 mg, 0.39 mmol, 1.0 equiv.) and  $\text{K}_2\text{CO}_3$  (161.71 mg, 1.17 mmol, 3.0 equiv.) in anhydrous acetonitrile (2 mL), CuI (37.14 mg, 0.20 mmol, 0.5 equiv.) and DMEDA (34.52 mg, 0.39 mmol, 1.0 equiv.) were added in a sealed tube under argon atmosphere. The mixture was heated at 100 °C for 12 h. The reaction was monitored by TLC. The mixture was filtered through a pad of Celite, and the residue was purified using silica chromatography. Yellow solid (122.74 mg, 133.73 mg), yield 62.5–68.1%.

**General procedure for synthesis of intermediates M8a–M8b.** To a solution of **M7a** or **M7b** (100 mg, 0.20 mmol, 1.0 equiv.) in THF and MeOH (2:1), iron powder (66.55 mg, 1.19 mmol, 6.0 equiv.) and AcOH (100  $\mu\text{L}$ ) were added under argon atmosphere. The mixture was stirred at 60 °C for 3 h. The reaction was monitored by TLC. The mixture was filtered through a pad of Celite, and the residue was purified using silica chromatography to obtain compounds **M8a–M8b** (69.61 mg, 72.07 mg). Yellow solid, yield 73.5–76.1%.

**General procedure for synthesis of compounds K16–K17.** The synthesis method of **K16–K17** was similar to **K01**.

**3-Amino-N-(3-(pyridin-3-ylethynyl)-1H-indazol-6-yl)benzenesulfonamide (K16).** Pale yellow solid (23.93 mg), yield 58.2%, m.p. 252.8–253.6 °C.  $^1\text{H}$  NMR (600 MHz, DMSO- $d_6$ )  $\delta$  13.39 (s, 1H), 10.42 (s, 1H), 8.84 (d,  $J = 1.4$  Hz, 1H), 8.61 (dd,  $J = 4.8, 1.3$  Hz, 1H), 8.07–8.04 (m, 1H), 7.73 (d,  $J = 8.7$  Hz, 1H), 7.49 (dd,  $J = 7.8, 4.9$  Hz, 1H), 7.29 (s, 1H), 7.13 (t,  $J = 7.9$  Hz, 1H), 7.04 (dd,  $J = 8.7, 1.5$  Hz, 1H), 6.97 (s, 1H), 6.88 (d,  $J = 7.8$  Hz, 1H), 6.70 (dd,  $J = 8.0, 1.6$  Hz, 1H), 5.58 (s, 2H).  $^{13}\text{C}$  NMR (151 MHz, DMSO- $d_6$ )  $\delta$  151.08, 148.81, 148.61, 139.81, 139.35, 138.02, 136.77, 128.98, 126.62, 123.06, 120.18, 119.78, 118.47,

117.10, 115.31, 112.62, 110.35, 99.16, 88.56, 83.94. HRMS (ESI,  $m/z$ ) calcd for  $C_{20}H_{15}N_5NaO_2S$   $[M + Na]^+$ : 412.0839; found: 412.0844.

*4-Amino-N-(3-(pyridin-3-ylethynyl)-1H-indazol-6-yl)*

*benzenesulfonamide (K17)*. Pale yellow solid (27.59 mg), yield 67.1%, m.p. 245.6–246.2 °C.  $^1H$  NMR (600 MHz, DMSO- $d_6$ )  $\delta$  13.33 (s, 1H), 10.15 (s, 1H), 8.84 (d,  $J = 2.0$  Hz, 1H), 8.62 (dd,  $J = 4.8, 1.4$  Hz, 1H), 8.06 (dt,  $J = 7.9, 1.7$  Hz, 1H), 7.70 (d,  $J = 8.7$  Hz, 1H), 7.49 (dd,  $J = 7.9, 4.9$  Hz, 1H), 7.41 (d,  $J = 8.7$  Hz, 2H), 7.27 (s, 1H), 7.01 (dd,  $J = 8.7, 1.5$  Hz, 1H), 6.52 (d,  $J = 8.7$  Hz, 2H), 5.98 (s, 2H).  $^{13}C$  NMR (151 MHz, DMSO- $d_6$ )  $\delta$  153.45, 152.15, 149.66, 140.95, 139.09, 138.31, 129.20 (2C), 127.65, 124.45, 124.13, 121.02, 120.73, 119.57, 116.29, 113.04 (2C), 99.76, 89.58, 85.08. HRMS (ESI,  $m/z$ ) calcd for  $C_{20}H_{15}N_5NaO_2S$   $[M + Na]^+$ : 412.0839; found: 412.0866. Retention time 2.975 min, HPLC purity = 99.66%.

**General procedure for synthesis of intermediates**

**M10a–M10b**. A mixture of **M9a** (1.0 g, 6.29 mmol, 1.0 equiv.) or **M9b** (1.0 g, 4.11 mmol, 1.0 equiv.) and (triisopropylsilyl) acetylene (3.0 equiv.) in dry TEA (10 ml) was degassed with argon for 3 min. Subsequently,  $PPh_3$  (0.1 equiv.) and  $Pd(OAc)_2$  (0.1 equiv.) were added. The mixture was stirred in a sealed tube at 100 °C for 4 h. Brown oil (948.57 mg, 925.56 mg), yield 57.9–65.3%.

**General procedure for synthesis of intermediates**

**M11a–M11b**. To a stirring solution of **M10a** (800 mg, 3.07 mmol, 1.0 equiv.) or **M10b** (800 mg, 2.32 mmol, 1.0 equiv.) in anhydrous THF (20 ml), TBAF (3.0 equiv.) was added at room temperature, and the mixture was stirred for 2 h. Pale yellow solid (171.32 mg, 263.83 mg), yield 53.6–60.1%.

**General procedure for synthesis of intermediates**

**M12a–M12b**. The synthesis method of **M12a–M12b** was similar to **M3**. Pale yellow solid (92.64 mg, 123.35 mg), yield 49.2–53.6%.

**General procedure for synthesis of intermediates**

**M13a–M13b**. The synthesis method of **M13a–M13b** was similar to **M4a–M4h**. Yellow solid (89.27 mg, 95.30 mg), yield 73.2–75.7%.

**General procedure for synthesis of intermediates**

**M14a–M14b**. The synthesis method of **M14a–M14b** was similar to **M8a–M8b**. Pale yellow solid (58.86 mg, 68.38 mg), yield 70.1–75.6%.

**General procedure for synthesis of compounds K20–K21**

The synthesis method of **K20–K21** was similar to **K01**. Pale yellow solid (22.64 mg, 20.86 mg), yield 50.7–53.3%.

*4-Amino-N-(3-((2-morpholinopyrimidin-5-yl)ethynyl)-1H-*

*indazol-6-yl)benzenesulfonamide (K20)*. Pale yellow solid (22.64 mg), yield 53.3%, m.p. 198.5–199.7 °C.  $^1H$  NMR (600 MHz, DMSO- $d_6$ )  $\delta$  13.21 (s, 1H), 10.12 (s, 1H), 8.65 (s, 2H), 7.65 (d,  $J = 8.7$  Hz, 1H), 7.40 (d,  $J = 8.8$  Hz, 2H), 7.24 (d,  $J = 1.1$  Hz, 1H), 6.98 (dd,  $J = 8.7, 1.7$  Hz, 1H), 6.51 (d,  $J = 8.8$  Hz, 2H), 5.97 (s, 2H), 3.78–3.76 (m, 4H), 3.68–3.66 (m, 4H).  $^{13}C$  NMR (151 MHz, DMSO- $d_6$ )  $\delta$  160.61 (3C), 159.74, 153.42, 140.92, 138.20, 129.19 (2C), 124.48, 120.85, 120.75, 116.05, 113.03 (2C), 106.19, 99.73, 88.03, 84.85, 66.35 (2C), 44.34 (2C). HRMS (ESI,  $m/z$ ) calcd for  $C_{23}H_{21}N_7NaO_3S$   $[M + Na]^+$ : 498.1319; found: 498.1359.

*4-Amino-N-(3-(pyrimidin-5-ylethynyl)-1H-indazol-6-yl)*

*benzenesulfonamide (K21)*. Pale yellow solid (20.86 mg), yield 50.7%, m.p. 281.5–282.2 °C.  $^1H$  NMR (600 MHz, DMSO- $d_6$ )  $\delta$  13.41 (s, 1H), 10.16 (s, 1H), 9.22 (s, 1H), 9.10 (s, 2H), 7.73 (d,  $J = 8.7$  Hz, 1H), 7.42 (d,  $J = 8.5$  Hz, 2H), 7.29 (s, 1H), 7.02 (d,  $J = 8.7$  Hz, 1H), 6.52 (d,  $J = 8.6$  Hz, 2H), 5.98 (s, 2H).  $^{13}C$  NMR (151 MHz, DMSO- $d_6$ )  $\delta$  159.23 (2C), 157.44, 153.45, 140.97, 138.39, 129.21 (2C), 127.22, 124.43, 121.08, 120.72, 119.11, 116.42, 113.04 (2C), 99.76, 88.48, 86.43. HRMS (ESI,  $m/z$ ) calcd for  $C_{19}H_{14}N_6NaO_2S$   $[M + Na]^+$ : 413.0801; found: 413.0815.

**General procedure for synthesis of compound M15**

3-Ethenylpyridine (168.12 mg, 1.60 mmol, 1.3 equiv.) was added to a solution of **M2** (2.00 g, 4.91 mmol, 1.0 equiv.) and DIEA (476.90 mg, 3.69 mmol, 3.0 equiv.) in anhydrous DMF (5 ml). The mixture was degassed with argon for 3 minutes, then tri(*o*-tolyl)phosphine (42.28 mg, 0.12 mmol, 0.1 equiv.) and  $Pd(OAc)_2$  (13.93 mg, 0.06 mmol, 0.05 equiv.) were added under argon atmosphere. The mixture was stirred at 100 °C for 4 h. The organic solvent removed under reduced pressure. The residue was purified using silica chromatography to obtain compound **M15**. Brown solid (289.27 mg), yield 61.2%.

**General procedure for synthesis of compound M16**

The synthesis method of **M16** was similar to **M7a–M7h**. Yellow solid (140.51 mg), yield 71.2%.

**General procedure for synthesis of compound M17**

The synthesis method of **M17** was similar to **M8a–M8b**. Pale yellow solid (70.64 mg), yield 75.1%.

**General procedure for synthesis of compound K22**

The synthesis method of **K22** was similar to **K01**.

*(E)-4-Amino-N-(3-(2-(pyridin-3-yl)vinyl)-1H-indazol-6-yl)*

*benzenesulfonamide (K22)*. Pale yellow solid (21.89 mg), yield 53.2%, m.p. 212.8–213.7 °C.  $^1H$  NMR (600 MHz, DMSO- $d_6$ )  $\delta$  12.98 (s, 1H), 10.06 (s, 1H), 8.84 (d,  $J = 1.7$  Hz, 1H), 8.45 (dd,  $J = 4.7, 1.4$  Hz, 1H), 8.13 (d,  $J = 8.0$  Hz, 1H), 8.03 (d,  $J = 8.7$  Hz, 1H), 7.58 (d,  $J = 16.8$  Hz, 1H), 7.45 (d,  $J = 16.8$  Hz, 1H), 7.42–7.39 (m, 3H), 7.22 (s, 1H), 6.97 (d,  $J = 8.7$  Hz, 1H), 6.51 (d,  $J = 8.1$  Hz, 2H), 5.96 (s, 2H).  $^{13}C$  NMR (151 MHz, DMSO- $d_6$ )  $\delta$  153.38, 148.83, 148.79, 142.41, 142.19, 137.66, 133.36, 133.05, 129.18 (2C), 126.35, 124.61, 124.23, 123.07, 121.82, 117.59, 115.49, 113.02 (2C), 99.80. HRMS (ESI,  $m/z$ ) calcd for  $C_{20}H_{17}N_5NaO_2S$   $[M + Na]^+$ : 414.0995; found: 414.1026. Retention time 5.624 min, HPLC purity = 97.45%.

## 4.2 Pharmacological assays

### 4.2.1 PLK4 LanthaScreen Eu kinase binding assay

The inhibitory activity test of the PLK4 enzyme was performed utilizing the LanthaScreen Eu kinase binding assay (Thermo Fisher Scientific) methodology, with **centrinone** (MedChemExpress, catalog No. HY-18682) serving as the positive control. The utilized instruments and components include: Tecan Infinite® F500 microplate reader, LanthaScreen Eu kinase binding assay kit (comprising Kinase

Tracer 236, Eu-Anti-GST Antibody, 1X Kinase Buffer A), 384-well shallow plates, and recombinant human PLK4 protein (amino acids 1–836, featuring a GST tag). The chemical sample was initially produced as a 10 mM solution utilizing DMSO. Subsequently, in accordance with the testing specifications, the compound was diluted with kinase buffer solution (1× kinase buffer A) to achieve working doses. In accordance with the operational manual, 4  $\mu\text{L}$  of the chemical sample was introduced into a 384-well plate, accompanied by 8  $\mu\text{L}$  of the kinase buffer solution containing recombinant human PLK4 kinase and Eu-anti-GST Antibody, as well as 4  $\mu\text{L}$  of the kinase buffer solution containing Tracer 236. The solution was incubated at ambient temperature for 60 minutes, and the plate was analyzed using a Tecan Infinite® F500 microplate reader at wavelengths of 665 and 615 nm.  $\text{IC}_{50}$  values were analyzed using GraphPad Prism 8, with each experiment conducted a minimum of two times.

**4.2.2 Cell proliferation assay.** Utilize the media suggested by the provider to cultivate the respective cell lines. The cell density ranges from 2000 to 6000 cells per well, injected into a 96-well plate containing 100  $\mu\text{L}$  of medium. Following a 24 hour incubation in humid air at 37 °C with 5%  $\text{CO}_2$ , the appropriate concentration of the drug was introduced to a 96-well plate and incubated for 5 days. Suspended cells were assessed for anti-proliferative activity utilizing the MTT assay (Beyotime, catalog no. ST316). Subsequently, the  $\text{IC}_{50}$  values were analyzed with GraphPad Prism 8.

**4.2.3 Colony-formation assay.** Inoculate MCF-7 cells at a density of 2000 cells per well in a six-well plate and incubate overnight in an incubator. After 24 hours, provide the appropriate concentration of the chemical or 0.1% DMSO to the cells. Replace the culture medium every three days. After 14 days, rinse the cells twice with PBS, fix them with formalin, and stain with crystal violet (Beyotime) for 10 minutes. Ultimately, rinse the surplus dye with distilled water, capture an image, and thereafter utilize ImageJ for quantification and analysis.

**4.2.4 Flow cytometry.** Inoculate the wells of a six-well plate with a cell density of  $2 \times 10^5$  cells per well. Subsequent to 24 hours, administer the appropriate concentration of DMSO or chemical to the cells for a duration of 48 hours. In the examination of apoptosis, gather the cells and resuspend them in phosphate-buffered saline (PBS). After spinning the cells in a centrifuge and using the annexin V-FITC apoptosis detection kit (Beyotime, catalog no. C1062M), look at the cells with a flow cytometer (BD Biosciences). In cell cycle analysis, gather the cells and resuspend them in cold phosphate-buffered saline (PBS). Centrifuge the cells and preserve them overnight at 4 °C using 70% ethanol. Eliminate the fixative and rinse the cells with PBS. After that, use the cell cycle and apoptosis analysis kit (Beyotime, catalog no. C1052) to stain the cells and a flow cytometer (BD Biosciences) to look at them.

### 4.3 Molecular docking

Utilize Schrödinger Maestro 12.8 software to investigate the binding mechanism of chemicals with PLK4 kinase. Initially, acquire the crystal structure of PLK4 (PDB code: 4JXF) from the Protein Data Bank (<https://www.rcsb.org/PDB>) and configure the PLK4 protein utilizing the Protein Preparation Wizard module with default parameters. Utilize the Glide module to delineate the binding location and dimensions (20 Å × 20 Å × 20 Å) according to the OPLS\_2005 force field. Utilize the LigPrep module to generate small molecule ligands employing the default parameters. Conduct molecular docking research with unrestricted docking and standard precision (SP) mode, employing Pymol software for visualization.

### 4.4 Plasma protein binding

Dissolve the compound to be tested in DMSO (10 mM). At the end of incubation, 10  $\mu\text{L}$  plasma sample was transferred from the donor side (in duplicate), added with 90  $\mu\text{L}$  PB (0.002% Tween-80) and vortexed well. 90  $\mu\text{L}$  of PB (0.002% Tween-80) sample was transferred from the receiver side (in duplicate), added with 10  $\mu\text{L}$  blank plasma and vortexed well. For recovery check, 10  $\mu\text{L}$  of the donor side loading sample was aliquoted into a 1.5 mL microcentrifuge tube (in duplicate), added with 90  $\mu\text{L}$  PB (0.002% Tween-80) and vortexed well. For stability check, 10  $\mu\text{L}$  of the donor side loading sample was aliquoted into a 1.5 mL microcentrifuge tube (in duplicate) at the end of incubation, added with 90  $\mu\text{L}$  PB (0.002% Tween-80) solution and vortexed well. Aliquots of 100  $\mu\text{L}$  of donor side, receiver side, stability and recovery samples were supplemented with 400  $\mu\text{L}$  of precipitant. After vortexing and centrifugation, 70  $\mu\text{L}$  of supernatant was removed and diluted with 70  $\mu\text{L}$  of water, vortexed well and aliquot of each solution was injected for LC-MS/MS analysis.

### 4.5 Liver microsomal stability

Dilute human, rat, and mouse liver microsomes (Corning, Lot No. 38295) to a concentration of 0.59 mg  $\text{mL}^{-1}$  to prepare the working solution. Transfer 445  $\mu\text{L}$  of the working solution to the preheated “incubation” plates T60 and NCF60, and shake at 37 °C for 10 minutes. After adding 5  $\mu\text{L}$  of the corresponding concentration of the compound and mixing thoroughly, take out 54  $\mu\text{L}$  of liver microsomes and transfer it to another black plate. Add 6  $\mu\text{L}$  of NADPH solution and 180  $\mu\text{L}$  of stop solution to the blackboard in sequence. Add 50  $\mu\text{L}$  of buffer to the NCF 60 plate and incubate with shaking at 37 °C for 60 minutes. Add 44  $\mu\text{L}$  of NADPH cofactor to the T60 plate and incubate at 37 °C for 60 minutes. At 5, 15, 30, 45, and 60 minutes, add 180  $\mu\text{L}$  of quenching solution to the plate, and at each time point, take out 60  $\mu\text{L}$  of the sample. Centrifuge at 4 °C at 4000 rpm for 20 minutes, transfer 20  $\mu\text{L}$  of the supernatant to 60  $\mu\text{L}$  of pure water, shake for 10 minutes, and then analyze using LC-MS/MS.

#### 4.6 Pharmacokinetic study

Single intravenous (1 mg kg<sup>-1</sup>) pharmacokinetic property studies on compound **K22** were performed in ICR mice ( $n = 3$ , pear group). After dosing blood (0.15 ml) collected from the jugular vein was taken at 0.083, 0.25, 0.5, 1, 2, 4, 8, and 24 h in an EDTA-K<sub>2</sub> nebulization tube. The blood samples were analyzed by LC-MS/MS.

### Abbreviations

DCM	Dichloromethane
DMF	<i>N,N</i> -Dimethylformamide
TEA	Triethylamine
DMEDA	<i>N,N'</i> -Dimethyl-1,2-ethanediamine
DHP	3,4-Dihydro-2 <i>H</i> -pyran
Pd <sub>2</sub> (dba) <sub>3</sub>	Tris(dibenzylideneacetone)dipalladium
Xantphos	4,5-Bis(diphenylphosphino)-9,9-dimethylxanthene

### Data availability

The data supporting this article have been included as part of the ESI.† All data in this study are real.

### Conflicts of interest

The authors declare no conflicts of interest.

### Acknowledgements

The Program for Innovative Research Team of the Ministry of Education and the Program for Liaoning Innovative Research Team in the University are gratefully acknowledged.

### References

- C.-H. Kim, D.-E. Kim and D.-H. Kim, *et al.*, Mitotic protein kinase-driven crosstalk of machineries for mitosis and metastasis, *Exp. Mol. Med.*, 2022, **54**, 414–425.
- S. C. Jana, J. F. Bazan and M. Bettencourt-Dias, Polo boxes come out of the crypt: a new view of PLK function and evolution, *Structure*, 2012, **20**(11), 1801–1804.
- Y. Zhao and X. Wang, PLK4: a promising target for cancer therapy, *J. Cancer Res. Clin. Oncol.*, 2019, **145**(10), 2413–2422.
- J. A. Winkles and G. F. Alberts, Differential regulation of polo-like kinase 1, 2, 3, and 4 gene expression in mammalian cells and tissues, *Oncogene*, 2005, **24**(2), 260–266.
- X. Zhang, C. Wei and H. Liang, *et al.*, Polo-Like Kinase 4's Critical Role in Cancer Development and Strategies for Plk4-Targeted Therapy, *Front. Oncol.*, 2021, **11**, 587554.
- R. Habedanck, Y.-D. Stierhof and C. J. Wilkinson, *et al.*, The Polo kinase Plk4 functions in centriole duplication, *Nat. Cell Biol.*, 2005, **7**(11), 1140–1146.
- Z. Li, K. Dai and C. Wang, *et al.*, Expression of Polo-Like Kinase 4(PLK4) in Breast Cancer and Its Response to Taxane-Based Neoadjuvant Chemotherapy, *J. Cancer*, 2016, **7**(9), 1125–1132.
- K. Shinmura, N. Kurabe and M. Goto, *et al.*, PLK4 overexpression and its effect on centrosome regulation and chromosome stability in human gastric cancer, *Mol. Biol. Rep.*, 2014, **41**(10), 6635–6644.
- Z. Liao, H. Zhang and P. Fan, *et al.*, High PLK4 expression promotes tumor progression and induces epithelial-mesenchymal transition by regulating the Wnt/beta-catenin signaling pathway in colorectal cancer, *Int. J. Oncol.*, 2022, **60**(1), 1.
- F. C. Kelleher, J. Kroes and J. Lewin, Targeting the centrosome and polo-like kinase 4 in osteosarcoma, *Carcinogenesis*, 2019, **40**(4), 493–499.
- G. M. Roberto, E. E. Engel and C. A. Scrideli, *et al.*, Downregulation of miR-10B\* is correlated with altered expression of mitotic kinases in osteosarcoma, *Pathol., Res. Pract.*, 2018, **214**(2), 213–216.
- A. W. Bailey, A. Suri and P. M. Chou, *et al.*, Polo-Like Kinase 4 (PLK4) Is Overexpressed in Central Nervous System Neuroblastoma (CNS-NB), *Bioengineering*, 2018, **5**(4), 96.
- R. A. Denu, M. Shabbir and M. Nihal, *et al.*, Centriole Overduplication is the Predominant Mechanism Leading to Centrosome Amplification in Melanoma, *Mol. Cancer Res.*, 2018, **16**(3), 517–527.
- M. Fischer, M. Quaas and A. Wintsche, *et al.*, Polo-like kinase 4 transcription is activated via CRE and NRF1 elements, repressed by DREAM through CDE/CHR sites and deregulated by HPV E7 protein, *Nucleic Acids Res.*, 2014, **42**(1), 163–180.
- C. Y. K. Chan, V. W. H. Yuen and D. K. C. Chiu, *et al.*, Polo-like kinase 4 inhibitor CFI-400945 suppresses liver cancer through cell cycle perturbation and eliciting antitumor immunity, *Hepatology*, 2023, **77**(3), 729–744.
- J. T. Pu, Z. Hu and D. G. Zhang, *et al.*, MiR-654-3p Suppresses Non-Small Cell Lung Cancer Tumourigenesis by Inhibiting PLK4, *Onco Targets Ther.*, 2020, **13**, 7997–8008.
- E. Ayoub, R. Heinz Montoya and V. Mohanty, *et al.*, Targeting Polo-like Kinase 4 Triggers Polyploidy and Apoptotic Cell Death in TP53-Mutant Acute Myeloid Leukemia, *Blood*, 2021, **138**, 1167–1167.
- R. R. Maniswami, S. Prashanth and A. V. Karanth, *et al.*, PLK4: a link between centriole biogenesis and cancer, *Expert Opin. Ther. Targets*, 2018, **22**(1), 59–73.
- F. Meitinger, M. Ohta and K.-Y. Lee, *et al.*, TRIM37 controls cancer-specific vulnerability to PLK4 inhibition, *Nature*, 2020, **585**(7825), 440–446.
- Z. Y. Yeow, B. G. Lambrus and R. Marlow, *et al.*, Targeting TRIM37-driven centrosome dysfunction in 17q23-amplified breast cancer, *Nature*, 2020, **585**(7825), 447–452.
- M. Marina and H. I. Saavedra, Nek2 and Plk4: prognostic markers, drivers of breast tumorigenesis and drug resistance, *Front. Biosci.-Landmark*, 2014, **19**(2), 352–365.
- A. Suri, A. W. Bailey and M. T. Tavares, *et al.*, Evaluation of Protein Kinase Inhibitors with PLK4 Cross-Over Potential in a Pre-Clinical Model of Cancer, *Int. J. Mol. Sci.*, 2019, **20**(9), 2112.

- 23 P. B. Sampson, Y. Liu and N. K. Patel, *et al.*, The discovery of Polo-like kinase 4 inhibitors: design and optimization of spiro[cyclopropane-1,3-[<sup>3</sup>H]indol]-2'(1'H)-ones as orally bioavailable antitumor agents, *J. Med. Chem.*, 2015, **58**(1), 130–146.
- 24 Q. Lei, L. Xiong and L. T. Yu, *et al.*, YLT-11, a novel PLK4 inhibitor, inhibits human breast cancer growth via inducing maladjusted centriole duplication and mitotic defect, *Cell Death Dis.*, 2018, **9**(11), 1066.
- 25 R. K. Tyler, N. Shpiro and R. Marquez, *et al.*, VX-680 inhibits Aurora A and Aurora B kinase activity in human cells, *Cell Cycle*, 2007, **6**(22), 2846–2854.
- 26 E. F. Johnson, K. D. Stewart and K. W. Woods, *et al.*, Pharmacological and functional comparison of the polo-like kinase family: insight into inhibitor and substrate specificity, *Biochemistry*, 2007, **46**(33), 9551–9563.
- 27 Y. L. Wong, J. V. Anzola and R. L. Davis, *et al.*, Reversible centriole depletion with an inhibitor of Polo-like kinase 4, *Science*, 2015, **348**(6239), 1155–1160.
- 28 Y. Sun, Y. Sun and L. Wang, *et al.*, Design, synthesis, and biological evaluation of novel pyrazolo [3,4-d]pyrimidine derivatives as potent PLK4 inhibitors for the treatment of TRIM37-amplified breast cancer, *Eur. J. Med. Chem.*, 2022, **238**, 114424.
- 29 Y. Xue, S. Mu and P. Sun, *et al.*, Design, synthesis, and biological evaluation of novel pyrimidin-2-amine derivatives as potent PLK4 inhibitors, *RSC Med. Chem.*, 2023, **14**(9), 1787–1802.
- 30 P. B. Sampson, Y. Liu and N. K. Patel, *et al.*, The Discovery of Polo-Like Kinase 4 Inhibitors: Design and Optimization of Spiro[cyclopropane-1,3'[<sup>3</sup>H]indol]-2'(1'H)-ones as Orally Bioavailable Antitumor Agents, *J. Med. Chem.*, 2015, **58**(1), 130–146.
- 31 S. Asha and M. Vidyavathi, Role of human liver microsomes in in vitro metabolism of drugs-a review, *Appl. Biochem. Biotechnol.*, 2010, **160**(6), 1699–1722.